FEBS openbio

FEBS PRESS science publishing by scientists

Diagnostic value of strand-specific miRNA-101-3p and miRNA-101-5p for hepatocellular carcinoma and a bioinformatic analysis of their possible mechanism of action

Xia Yang[1,†], Yu-Yan Pang[1,†], Rong-Quan He[2], Peng Lin[3], Jie-Mei Cen[2], Hong Yang[3], Jie Ma[2,#] and Gang Chen[1,#]

1 Department of Pathology, First Affiliated Hospital of Guangxi Medical University, Nanning, China
2 Department of Medical Oncology, First Affiliated Hospital of Guangxi Medical University, Nanning, China
3 Department of Ultrasonography, First Affiliated Hospital of Guangxi Medical University, Nanning, China

Keywords
bioinformatics; Gene Expression Omnibus; hepatocellular carcinoma; microRNA-101-3p; microRNA-101-5p; The Cancer Genome Atlas

Correspondence
J. Ma, Department of Medical Oncology, First Affiliated Hospital of Guangxi Medical University, Shuangyong Road 6, Nanning, Guangxi, China
Tel: +86 771 5312980
E-mail: majie086@163.com
G. Chen, Department of Pathology, First Affiliated Hospital of Guangxi Medical University, Shuangyong Road 6, Nanning, Guangxi, China
Tel: +86 771 5356534
E-mail: chen_gang_triones@163.com

[†]These authors contributed equally to this work.
[#]These authors contributed equally to this work.

(Received 19 March 2017, revised 8 May 2017, accepted 8 November 2017)

doi:10.1002/2211-5463.12349

There is accumulating evidence that miRNA might serve as potential diagnostic and prognostic markers for various types of cancer. Hepatocellular carcinoma (HCC) is the most common type of malignant lesion but the significance of miRNAs in HCC remains largely unknown. The present study aimed to establish the diagnostic value of miR-101-3p/5p in HCC and then further investigate the prospective molecular mechanism via a bioinformatic analysis. First, the miR-101 expression profiles and parallel clinical parameters from 362 HCC patients and 50 adjacent non-HCC tissue samples were downloaded from The Cancer Genome Atlas (TCGA). Second, we aggregated all miR-101-3p/5p expression profiles collected from published literature and the Gene Expression Omnibus and TCGA databases. Subsequently, target genes of miR-101-3p and miR-101-5p were predicted by using the miRWalk database and then overlapped with the differentially expressed genes of HCC identified by natural language processing. Finally, bioinformatic analyses were conducted with the overlapping genes. The level of miR-101 was significantly lower in HCC tissues compared with adjacent non-HCC tissues ($P < 0.001$), and the area under the curve of the low miR-101 level for HCC diagnosis was 0.925 ($P < 0.001$). The pooled summary receiver operator characteristic (SROC) of miR-101-3p was 0.86, and the combined SROC curve of miR-101-5p was 0.80. Bioinformatic analysis showed that the target genes of both miR-101-3p and miR-101-5p are involved in several pathways that are associated with HCC. The hub genes for miR-101-3p and miR-101-5p were also found. Our results suggested that both miR-101-3p and miR-101-5p might be potential diagnostic markers in HCC, and that they exert their functions via targeting various prospective genes in the same pathways.

Abbreviations
AFP, alpha-fetoprotein; AUC, area under the curve; BP, biological process; CC, cellular component; CI, confidence interval; CNKI, Chinese National Knowledge Infrastructure; DAVID, Database for Annotation, Visualization and Integrated Discovery; FN, false negative; FoxO, forkhead box O; FP, false positive; GEO, Gene Expression Omnibus; GO, Gene Ontology; HBV, hepatitis B virus; HCC, hepatocellular carcinoma; KEGG, Kyoto Encyclopedia of Genes and Genomes; MAPK, mitogen-activated protein kinase; MF, molecular function; NLP, natural language processing; NLR, negative likelihood ratio; PI3K, phosphoinositide-3-kinase; PLR, positive likelihood ratio; PPI, protein–protein interaction; pre-miRNA, precursor miRNA; ROC, receiver operating characteristic; SROC, summary receiver operator characteristic; TCGA, The Cancer Genome Atlas; TN, true negative; TP, true positive.

According to Cancer Statistics, 2017 [1], the incidence rates of liver cancer in the USA continue to increase rapidly (~ 3% per year in women and 4% per year in men), and the death rate rose by almost 3% per year from 2010 to 2014. In addition, the mortality rate is three times higher in men than in women. Since Asia is the area with the highest incidence rate of liver cancer, especially China, annual incidence and mortality are more than half of the global totals [2]. Among the three histological types of liver malignancy, hepatocellular carcinoma (HCC) has become the leading cause of death from cancer. Since there have been no biomarkers or common surgical techniques for the early stage of HCC, the majority of patients with HCC are diagnosed late, which directly correlates with a poor outcome and low survival rate. As with other cancers, HCC development is a multistep process with abundant genetic and epigenetic mutations. A recent study confirmed that hepatocarcinogenesis can be caused by chronic hepatitis B virus (HBV) infection [3]. Much effort towards the treatment of HBV-infected HCC has been made in the past, but with only limited success. Thus, identifying novel biochemical markers for early HCC diagnosis is a matter of the utmost urgency.

miRNAs, ~ 20–22 nucleotides in length, are a class of small endogenous non-coding RNA molecules. They post-transcriptionally regulate mRNA expression through imperfect base paring with the 3′-untranslated region of target genes. With comprehensive study, miRNAs have become known as the star molecules of cancer research. miRNAs in human cancers are involved in several pivotal biological processes (BP), including cancer proliferation, differentiation, progression and cell apoptosis [4–6]. Although their functions remain elusive, up- and down-regulation of miRNAs have been widely reported in all kinds of cancer tissues in comparison with expression in the corresponding normal tissues [7,8]. In particular, miRNAs have been found to be biomarkers for cancer clinical diagnosis, histological classification and prognosis [9–13].

Accumulating evidence has clearly demonstrated that the aberrant expression of miRNAs may further influence the expression of tumor oncogenes and suppressor genes, thereby leading to the occurrence of a tumor [14–17]. Theoretically, mature miRNA generation requires a series of enzyme reactions. First, primary miRNA transcripts are cleaved in the nucleus by the Drosha enzyme to liberate the precursor miRNA (pre-miRNA) hairpin. Subsequently, the pre-miRNA is exported to the cytoplasm and further processed by the enzyme Dicer to produce two mature miRNAs (miR-5p and miR-3p) [18,19]. Even though the two mature miRNAs are transcribed from the same pre-miRNA, they may have different target genes and biological functions. A previous study [20] reported that the expression levels of the miR-5p and miR-3p mature sequences can be altered in different tissues.

Accumulating evidence [19,21–25] has shown that miR-101-3p/-5p is down-regulated in multiple malignances, including HCC. For example, Hou *et al.* [26] explored miRNA expression profiling and revealed that miR-101 (3p and 5p were not distinguished) expression in HCC tissues was lower than in healthy controls. Wei *et al.* [27] also showed that miR-101 (3p and 5p were not distinguished) was down-regulated in HBV-associated HCC tissues and may have therapeutic potential in HCC. Additionally, the function of these miRNAs has also been investigated. Zhang *et al.* [28] revealed that enforced expression of miR-101 (3p and 5p were not distinguished) by siRNA inhibited the cell proliferation and tumorigenicity of an HCC cell line *in vitro*. Sheng *et al.* [29] investigated how miR-101-3p regulated cell proliferation, cell cycle and apoptosis in HCC and found that overexpression of miR-101-3p caused an enhanced rate of apoptosis but no obvious change in the cell cycle. Besides, several oncogenes, such as *EZH2*, *FOS*, *COX-2* and *SOX9*, have been found to be directly regulated by miR-101-3p/5p [30–32]. Recently the potential of the miR-101 family as diagnostic indicators has also caught the eye of researchers. He *et al.* [33] conducted a meta-analysis that summarized miRNAs' diagnostic value in HCC and found that miR-101-5p had great diagnostic value, though only three data sets were included and the results need to be further validated. Furthermore, in human, miR-101 precursor transcripts are encoded with two genomic loci (miR-101-1 and miR-101-2). For two mature miRNAs, miR-101-3p is generated from the 3′ ends of the precursors, and miR-101-5p from the 5′ end of pre-miR-101-1 (http://www.mirbase.org/). We speculated that miR-101-3p may also serve as a diagnostic marker for HCC. Since the seed region of miR-101-3p and miR-101-5p is unique, they are predicted to regulate unique targets. However, to the best of our knowledge, the comparative roles of miR-101-3p and miR-101-5p in HCC have not yet been fully studied.

The present study investigated miR-101-3p and miR-101-5p expression in HCC tissues compared with that in healthy controls. Published studies, Gene Expression Omnibus (GEO) microarray chips and The Cancer Genome Atlas (TCGA) data that included miR-101-3p or miR-101-5p expression information were collected together. Additionally, previous studies have mainly focused on a single gene [34–36], and studies have rarely focused on the function of

coexpressed genes in cancers. For the purpose of obtaining a full understanding of the molecular mechanisms underlying HCC, comprehensive bioinformatics methods were used to investigate the function and pathways of target genes of miR-101-3p and miR-101-5p associated with HCC. In a word, the present study aimed to analyze the expression and mechanism of miR-101-3p and miR-101-5p in the initiation and development of HCC. This exploration will provide novel insights into HCC. A flowchart for the whole study designed is shown in Fig. 1.

Material and methods

The clinical role of miR-101 based on the public database TCGA

To verify the difference in the miR-101 expression levels between HCC and normal liver tissues, we downloaded relevant data from the public tumor database TCGA, in which samples from 362 HCC patients and 50 adjacent non-HCC tissues were included. Additionally, miR-101-1 and miR-101-2 levels were both calculated because the relevant sample data were provided in TCGA. miR-101-1 and miR-101-2 are two precursor hairpin structures of miR-101 miRNA that are located in the human genome on chromosome 1 (MI0000103) and 9 (MI0000739), respectively [37]. Both of them are processed by the Dicer enzyme to form the mature miRNA. All of the available clinical parameters were analyzed by SPSS STATISTICS 22.0 (IBM Corp., Armonk, NY, USA).

Data mining

Search strategy and study selection

Comprehensive literature searches were conducted on electronic databases PubMed, EMBASE, Web of Science, the Cochrane Library, and Chinese National Knowledge Infrastructure (CNKI) up to 29 December 2016. No language limitations were imposed. Qualifying articles were screened by combining the following keywords: 'miR-101' OR 'miRNA-101' OR 'miRNA-101' OR 'miR101' OR 'miRNA101' OR 'miRNA 101' OR 'miR-101-5p' OR 'miRNA-101-5p' OR 'miRNA-101-5p' OR'miR-101-3p' OR 'miRNA-101-3p' OR 'miRNA-101-3p' AND malignan* OR cancer OR tumor OR neoplas* OR carcinoma AND hepatocellular OR liver OR hepatic OR HCC AND diagnos* OR receiver operating characteristic (ROC) OR specificity OR sensitivity OR DEGs OR DEMs OR 'differentially expressed'. In addition, the reference lists were also manually searched to reduce article omission. The title and abstract of the obtained studies were scanned to exclude any clearly irrelevant publications. In addition to searching the literature, we also searched the GEO database for eligible microarrays with the following terms: malignan* OR

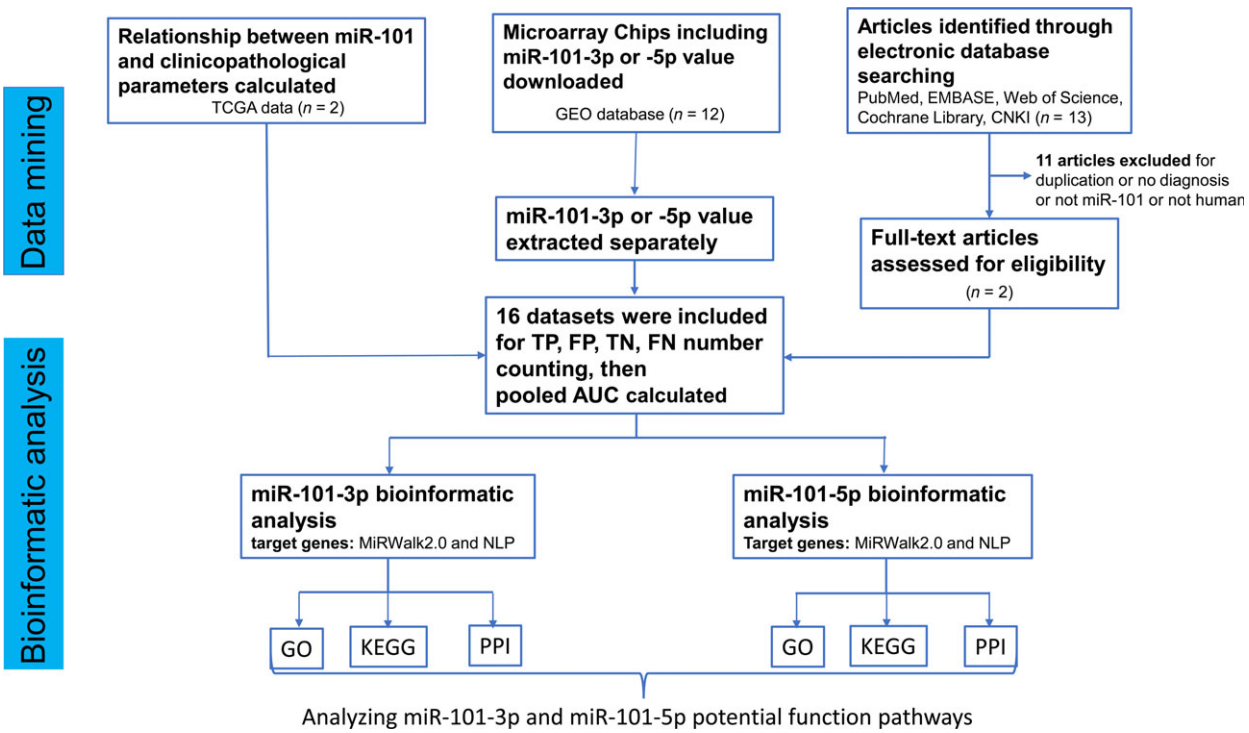

Fig. 1. Flowchart of the study design.

cancer OR tumor OR neoplas* OR carcinoma AND hepatocellular OR liver OR hepatic OR HCC.

Criteria for inclusion and exclusion

Studies that met the following criteria were included: (a) investigated HCC; (b) measured the level of miR-101, miR-101-3p or miR-101-5p in HCC tissue, plasma or serum; (c) included the diagnosis of HCC or the clinical parameters; and (d) reported true positives (TPs), false positives (FPs), false negatives (FNs), and true negatives (TNs) or sensitivity and specificity of miR-101. In addition, (e) if the studies did not provide a fourfold contingency table, they were included if the original data were available; and (f) microarrays were included if they enrolled more than three patient samples and measured the miR-101 profile for HCC.

Articles that met the following criteria were excluded: (a) studies without sufficient data, such as reviews or systematic reviews, (b) repeat reports, (c) studies conducted on cell lines or animals and (d) letters to the editor or conference abstracts.

Data synthesis and analysis

Studies that did not provide TPs, FPs, FNs and TNs but gave sensitivity and specificity or the original data were translated by MEDCALC 11.4.2.0 (MedCalc Software, Ostend, Belgium). To reduce inaccuracy in the relevant data extracted from the included studies, three independent researchers (XY, PL and JMC) performed the data extraction separately.

Statistical analysis

All statistical analyses were performed using SPSS STATISTICS 20.0 or STATA 12.0 (StataCorp, College Station, TX, USA). For the clinical parameter analysis, miR-101 expression was represented as the mean ± standard deviation. The standards for assessing the area under the curve (AUC) in the ROC curve were as follows: 0.5–0.7 represented poor evidence for diagnosis, 0.7–0.9 represented moderate evidence for diagnosis and 0.9–1.0 represented high evidence for diagnosis. The correlation between miR-101 expression and the clinicopathological parameters was investigated with Spearman's rank correlation. The significance of the difference between HCC and non-cancerous liver tissues was studied using Student's *t* test. The significant differences among three groups were examined by one-way ANOVA. For data mining, the pooled sensitivity, specificity, positive likelihood ratios (PLRs), negative likelihood ratios (NLRs), and diagnostic odds ratio with their corresponding 95% confidence intervals (CIs) were calculated with the bivariate regression model. Additionally, the

Table 1. Relationship between miR-101-1 and clinicopathological parameters in HCC (TCGA data).

	miR-101-1 relative expression				Correlation analysis	
Clinicopathological feature	*n*	Mean ± SD	*t*	*P*	*r*	*P*
Tissue						
HCC	362	15.25 ± 1.05	−16.198	0.000	0.480	0.000
Normal	50	16.93 ± 0.62				
Gender						
Male	247	15.23 ± 1.03	−0.542	0.588	0.015	0.774
Female	115	15.29 ± 1.09				
Age						
< 50 years	68	15.06 ± 1.13	−1.708	0.089	0.031	0.559
≥ 50 years	290	15.30 ± 1.03				
HBV						
−	255	15.20 ± 1.08	1.347	0.179	0.079	0.133
+	106	15.37 ± 0.98				
HCV						
−	308	15.22 ± 1.05	1.407	0.160	0.054	0.309
+	54	15.44 ± 1.01				
Pathological stage						
Stage I–II	250	15.34 ± 1.01	3.276	0.001	−0.174	0.001
Stage III–IV	88	14.92 ± 1.16				
Pathological T						
T1–T2	268	15.33 ± 1.01	2.867	0.004	−0.173	0.001
T3–T4	92	14.97 ± 1.12				
Histological grade						
GI–II	223	15.40 ± 1.05	3.467	0.001	−0.184	0.000
GIII–IV	135	15.00 ± 1.02				

Table 2. Relationship between miR-101-2 and clinicopathological parameters in HCC (TCGA data).

	miR-101-2 relative expression				Correlation analysis	
Clinicopathological feature	*n*	Mean ± SD	*t*	*P*	*r*	*P*
Tissue						
HCC	362	15.27 ± 1.05	−16.256	0.000	0.481	0.000
Normal	50	16.94 ± 0.61				
Gender						
Male	247	15.25 ± 1.03	−0.533	0.594	0.016	0.760
Female	115	15.31 ± 1.09				
Age						
< 50 years	68	15.08 ± 1.13	−1.709	0.088	0.032	0.550
≥ 50 years	290	15.32 ± 1.03				
HBV						
−	255	15.22 ± 1.07	1.347	0.179	0.079	0.133
+	106	15.39 ± 0.98				
HCV						
−	308	15.24 ± 1.05	1.425	0.155	0.054	0.309
+	54	15.46 ± 1.01				
Pathological stage						
Stage I–II	250	15.36 ± 1.01	3.309	0.001	−0.174	0.001
Stage III–IV	88	14.93 ± 1.15				
Pathological T						
T1–T2	268	15.35 ± 1.00	2.904	0.004	−0.174	0.001
T3–T4	92	14.99 ± 1.12				
Histological grade						
GI–II	223	15.41 ± 1.04	3.452	0.001	−0.184	0.000
GIII–IV	135	15.03 ± 1.02				

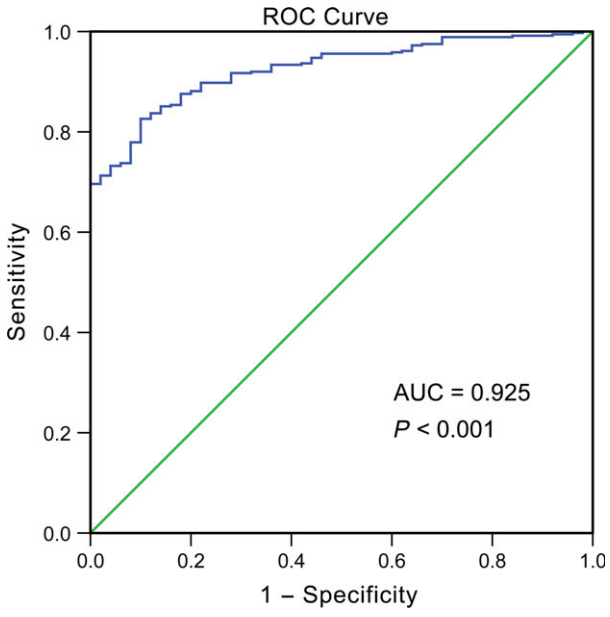

Fig. 2. MiR-101 expression profiles for the diagnosis of HCC. The AUC of the low miR-101 level for HCC diagnosis was 0.925 (95% CI: 0.896–0.953, $P < 0.001$).

summary receiver operator characteristic (SROC) curve with the area under the SROC curve was calculated [38]. What is more, the Q test and the I^2 measure of inconsistency were used to quantify heterogeneity between studies [39]. The possibility of publication bias was finally explored by Deeks' funnel plot, and P values < 0.1 were considered significant.

Bioinformatic analysis

In silico analysis of target genes of miR-101

MiRWalk2.0 [40] (http://zmf.umm.uni-heidelberg.de/apps/zmf/mirwalk2/), which combines 12 existing miRNA-target prediction programs, was used to provide comprehensive potential targets for miR-101-3p and miR-101-5p. The genes identified by more than eight prediction software programs for miR-101-3p and more than six for miR-101-5p were selected to obtain more reliable targets.

Natural language processing

Natural language processing (NLP) is a novel computerized approach to analyze electronic free text to achieve 'human-like language processing'. With this approach, programmers create software to 'read' text and extract key pieces of information from clinician notes, procedure/radiology/pathology reports and laboratory results [41,42]. We performed a literature search in PubMed to obtain all related electronic records. The detailed process was described in

our previous article [43,44]. Finally, 1800 genes that were differentially expressed in HCC were identified for further analysis.

Functional and signaling pathway analyses

A set of condition-specific genes from the overlapping genes from the target prediction software and NLP further underwent functional and signaling pathway analyses on a public database platform, the Database for Annotation, Visualization and Integrated Discovery (DAVID; https://david.ncifcrf.gov/), which provides a functional interpretation of massive gene lists derived from genomic studies. The analyses included Gene Ontology (GO) function analysis (http://www.geneontology.org/) and Kyoto Encyclopedia of Genes and Genomes (KEGG; http://www.genome.jp/kegg/) analysis. The GO function analysis categorized selected genes into groups in accordance with three independent classification standards, BPs, cellular components (CCs), and molecular functions (MFs). The top 10 terms of each GO category and top 30 pathways of the KEGG pathways were visualized as GO maps and KEGG maps, separately, via CYTOSCAPE v3.4.0 (http://cytoscape.org/).

Protein–protein interaction network construction

Overlapping genes were inputted to the STRING v10.0 online tool (http://string-db.org/) to construct the protein–protein interaction (PPI) network. The direct (physical) and indirect (functional) associations of proteins were derived from four methods: (a) literature-reported protein interactions, (b) high-throughput experiments, (c) genome analysis and

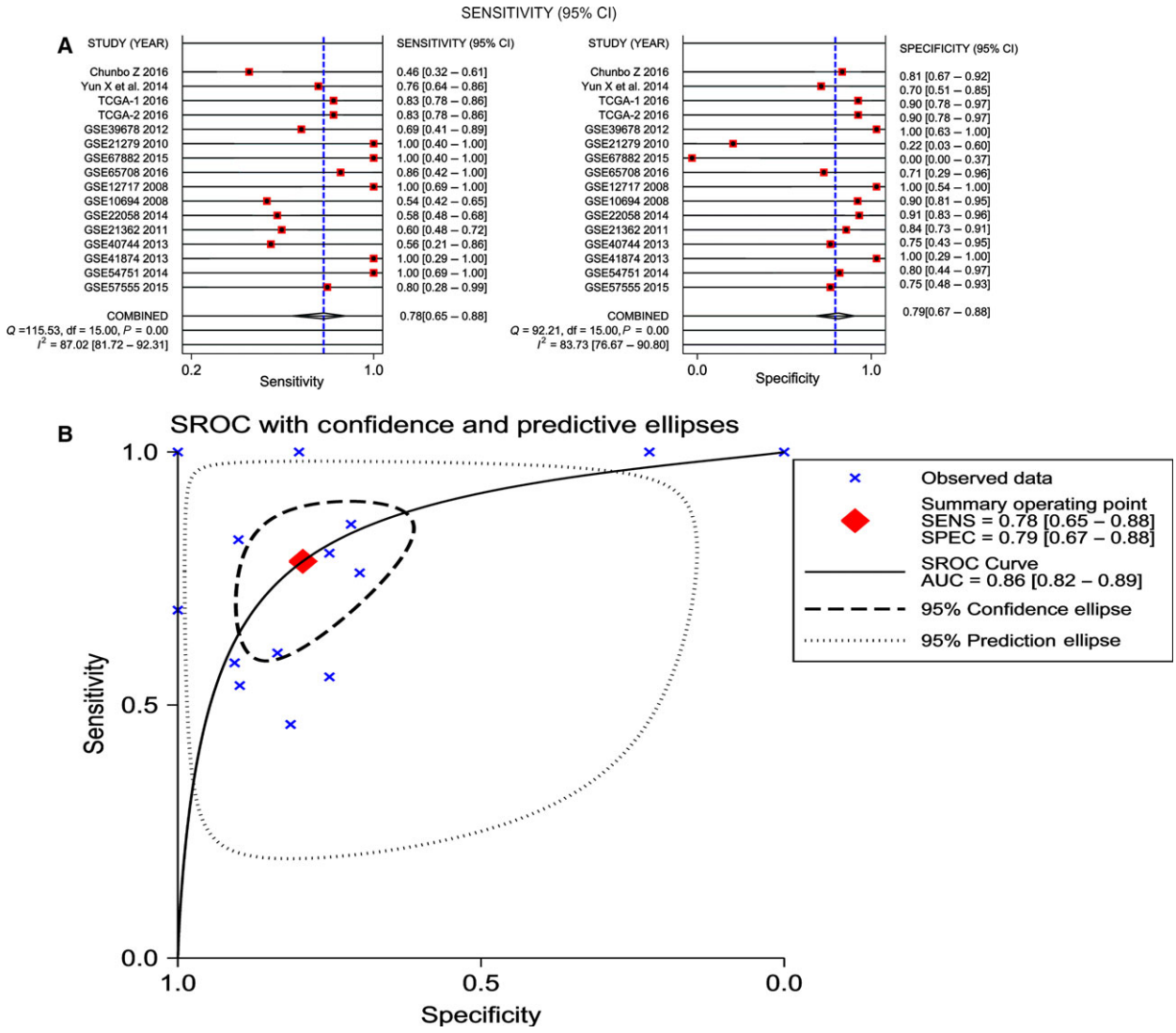

Fig. 3. Diagnostic accuracy of miR-101-3p in HCC. (A) Sensitivity (SENS) and specificity (SPEC) with corresponding heterogeneity statistics. (B) SROC curves for miR-101-3p with CI in the diagnosis of HCC.

prediction and (d) coexpression studies. By scrutinizing the connectivity degrees of the nodes in the PPI networks, we determined the hub genes. A node with a high degree of connectivity is perceived as a hub node.

Results

Clinicopathological significance of miR-101-1/miR-101-2 in HCC tissues

The relationship between miR-101-1/miR-101-2 and clinicopathological parameters in HCC was mined from TCGA, as shown in Tables 1 and 2. Data profiling revealed that when compared with the expression in para-non-cancerous normal tissues (16.93 ± 0.62), miR-101-1 expression was significantly reduced in HCC tissues (15.25 ± 1.05, $P < 0.001$). In addition, the AUC of the low miR-101-1 level for HCC diagnosis was 0.925 (95% CI: 0.896–0.953, $P < 0.001$, Fig. 2) with a cut-off value of 16.17 (82.6% sensitivity and 90.0% specificity). Similar results were also obtained for miR-101-2 (15.27 ± 1.05 in HCC and 16.94 ± 0.61 in para-non-cancerous liver tissues, $P < 0.001$). Additionally, the altered expressions of miR-101-1 and miRNA-101-2 were both associated with pathological stage, pathological T stage and histological stage. Compared with the expression in advanced stage (III and IV) HCC patients, the relative expression of miR-101 in early stage patients was notably increased (I and II, $P < 0.05$), and the Spearman correlation test confirmed that the correlations between miR-101 and the pathological stage, pathological T stage and histological stage were $r = -0.17$, $P = 0.001$; $r = -0.17$, $P = 0.001$ and $r = -0.18$, $P < 0.001$, respectively.

Diagnostic value of miR-101-3p and miR-101-5p

Study selection

Through the literature search, 341 relevant articles were identified, 339 of which were excluded for being case reports, reviews, letters, repeat publications and

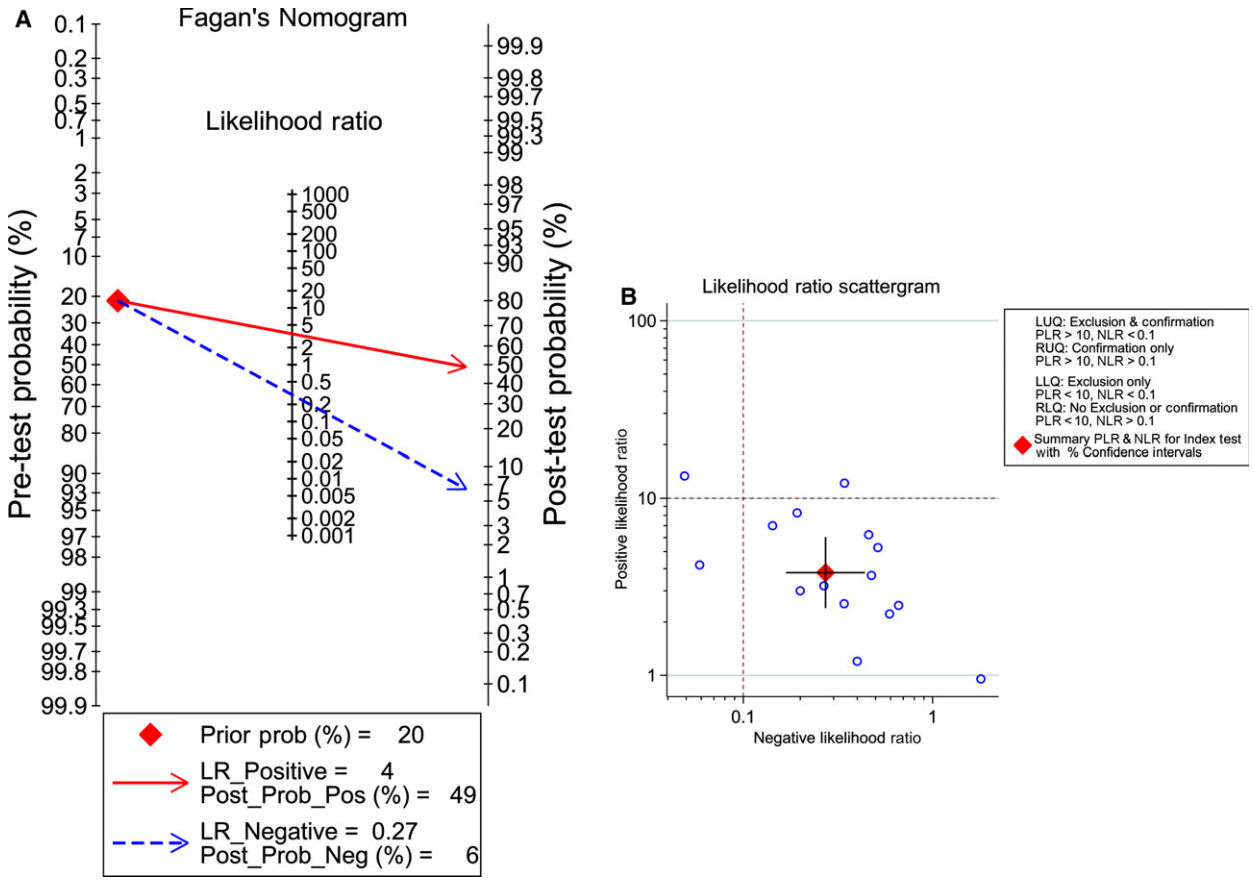

Fig. 4. Fagan diagram and likelihood matrix for miR-101-3p to diagnose cancer or to eliminate the diagnosis of cancer. (A) Pre-test probability of the miR-101-3p assay in HCC detection. (B) Likelihood matrix showing individual (circles) and pooled (diamond) values of PLRs combined with NLRs. LLQ, left lower quadrant; LUQ, left upper quadrant; RLQ, right lower quadrant; RUQ, right upper quadrant.

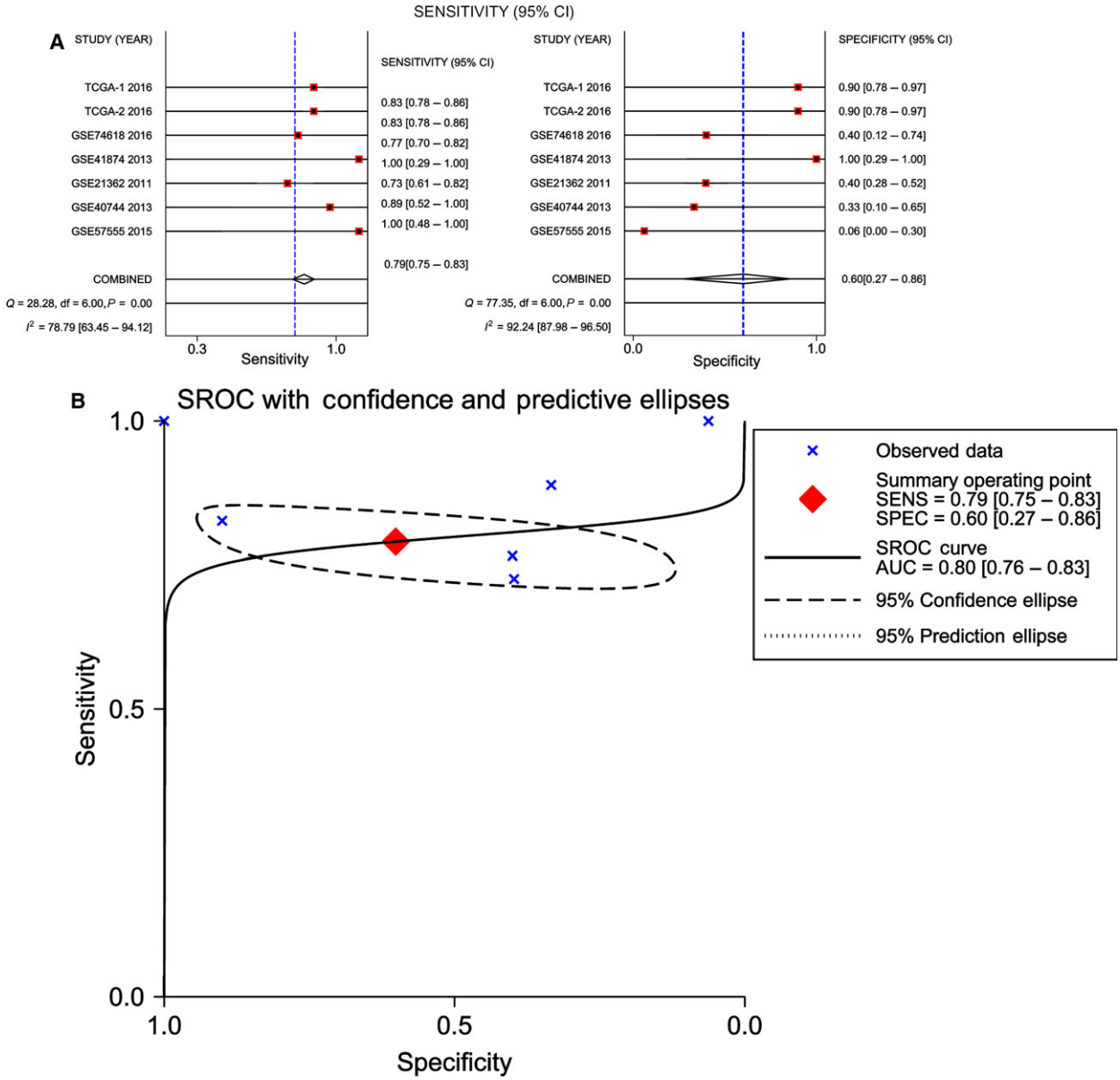

Fig. 5. Diagnostic accuracy of miR-101-5p in HCC. (A) Sensitivity (SENS) and specificity (SPEC) with corresponding heterogeneity statistics. (B) SROC curves for miR-101-5p with CI in the diagnosis of HCC.

studies not specifically pertaining to miR-101-3p/5p. The two remaining publications were examined by three researchers and ultimately included. Moreover, GEO microarrays that detected miR-101-3p and/or miR-101-5p were identified for further analysis and were combined after assessment. Finally, 12 datasets including 315 HCC and 330 normal control samples were downloaded from the GEO database to calculate the miR-101-3p diagnostic value (GSE39678, GSE21279, GSE67882, GSE65708, GSE12717, GSE 10694, GSE22058, GSE21362, GSE40744, GSE41874, GSE54751 and GSE57555); five datasets including 308 HCC and 114 normal control samples were downloaded from the GEO database to calculate the miR-101-5p diagnostic value (GSE74618, GSE21362, GSE40744, GSE41874 and GSE57555). In addition, the precursors of miR-101 identified from TCGA were also considered.

Heterogeneity analysis

The analysis of heterogeneity is widely used to evaluate the accuracy of statistical pooling from multiple studies [45]. Since heterogeneities may come

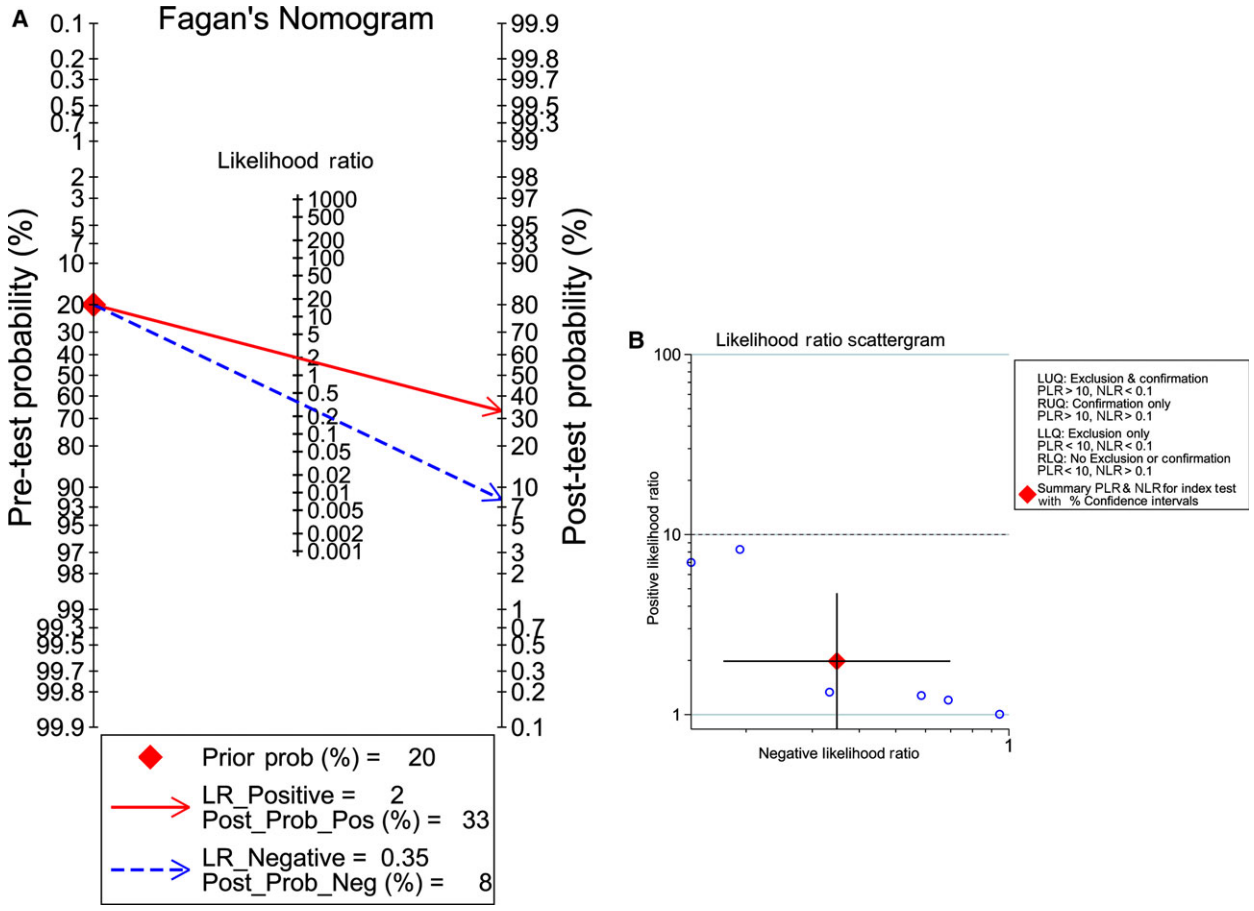

Fig. 6. Fagan diagram and likelihood matrix for miR-101-5p to diagnose cancer or to eliminate the diagnosis of cancer. (A) Pre-test probability of the miR-101-5p assay in HCC detection. (B) Likelihood matrix showing individual (circles) and pooled (diamond) values of PLRs combined with NLRs. LLQ, left lower quadrant; LUQ, left upper quadrant; RLQ, right lower quadrant; RUQ, right upper quadrant.

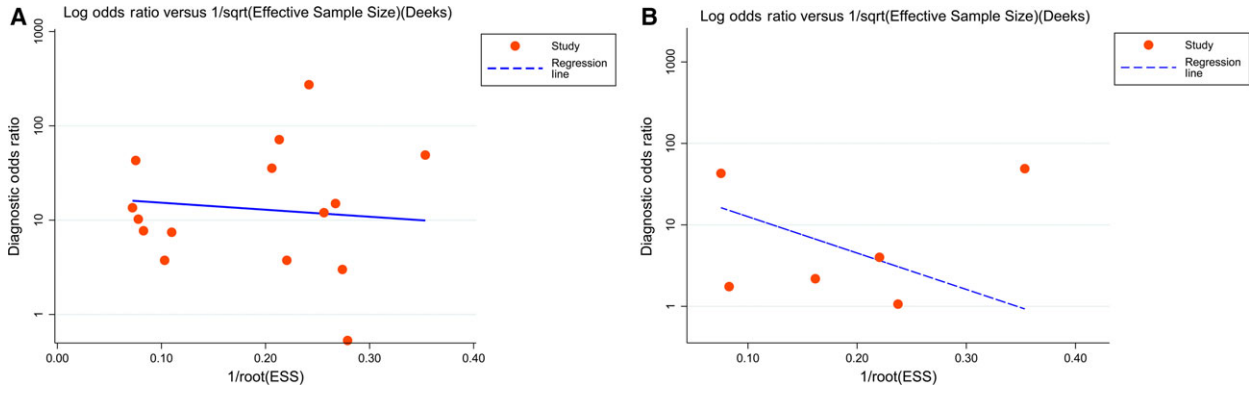

Fig. 7. The Deeks' test that assesses potential publication bias in the miR-101 assay. (A) Potential publication bias assessment of miR-101-3p. (B) Potential publication bias assessment of miR-101-5p.

from a threshold effect and a non-threshold effect, the threshold effect was first explored by the Spearman test to calculate the heterogeneity of miR-101-3p/5p among the included studies. In other words, the correlation coefficient and *P* value between the logit of sensitivity and logit of 1 – specificity were calculated. As

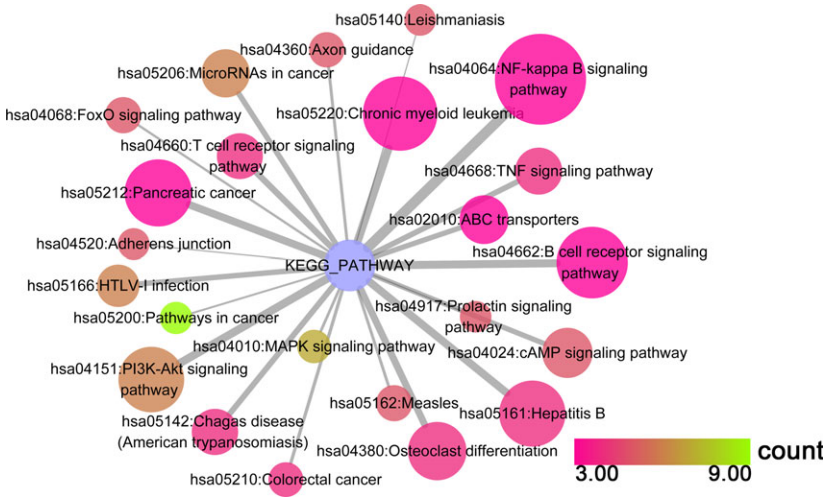

Fig. 8. The KEGG pathway analysis of miR-101-3p predicted target genes in HCC. Pathway analyses were performed to identify significantly enriched pathways by using CYTOSCAPE v3.4.0. The top 30 pathways are displayed; the map node size represents the *P* value of targets, low values are indicated by large nodes, and the node color represents the gene count number with low values indicated by pink.

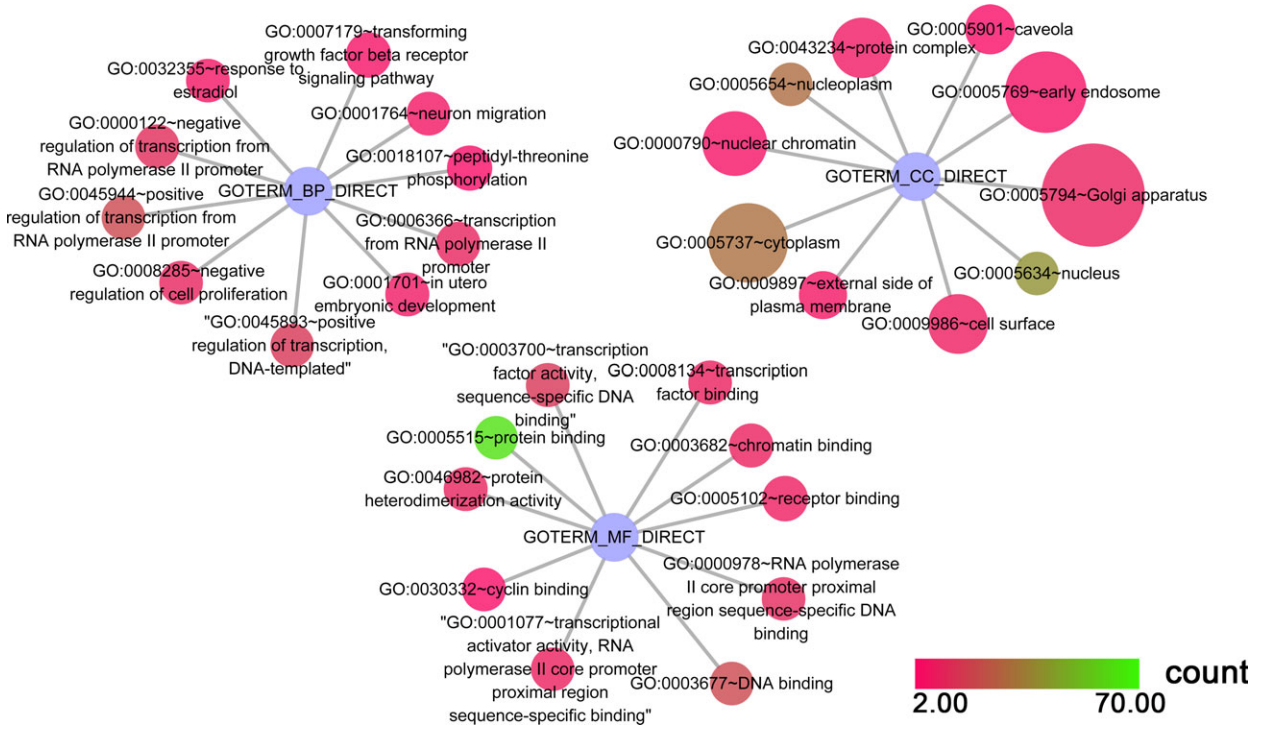

Fig. 9. The KEGG pathway analysis of miR-101-5p predicted target genes in HCC. Pathway analyses were performed to identify significantly enriched pathways by using CYTOSCAPE v. 3.4.0. The top 30 pathways are displayed; the map node size represents the *P* value of targets, low values are indicated by large nodes, and the node color represents the gene count number with low values indicated by pink.

a result, the Spearman correlation coefficients for miR-101-3p and miR-101-5p were 0.386 ($P = 0.215$) and −0.059 ($P = 0.912$), respectively, indicating that heterogeneity from the threshold effect was not found. However, the I^2 values in the forest plots of sensitivity and specificity (more than 50%) revealed that we cannot ignore the non-threshold effect from the included studies.

Diagnostic accuracy of miR-101-3p and miR-101-5p in HCC

Evident heterogeneity for pooled sensitivity and specificity of miR-101-3p was seen in the collected data ($I^2 = 87.02\%$ and 83.73%, respectively, $P < 0.05$); thus, a random effects model was finally selected, based on which the pooled sensitivity and specificity of

Table 3. KEGG functional annotation for most significantly related targets of miR-101.

KEGG ID	Term	Gene no.	*P*	Genes
MiR-101-3p				
hsa04520	Adherens junction	5	8.53×10^{-4}	MAP3K7, MAPK1, TGFBR1, NLK, SSX2IP
hsa05140	Leishmaniasis	5	8.53×10^{-4}	MAP3K7, MAPK1, FOS, PTGS2, JAK2
hsa04917	Prolactin signaling pathway	5	8.53×10^{-4}	MAPK1, FOS, SOCS2, GSK3B, JAK2
hsa05200	Pathways in cancer	9	2.18×10^{-3}	CEBPA, MAPK1, FOS, PTGS2, TGFBR1, GSK3B, PTCH1, CDK6, CXCL12
hsa04010	MAPK signaling pathway	7	4.09×10^{-3}	MAP3K7, MAPK1, FOS, DUSP1, TGFBR1, NLK, SRF
hsa05210	Colorectal cancer	4	6.16×10^{-3}	MAPK1, FOS, TGFBR1, GSK3B
hsa04360	Axon guidance	5	7.10×10^{-3}	MAPK1, EPHA7, NRP1, GSK3B, CXCL12
hsa05162	Measles	5	8.34×10^{-3}	MAP3K7, GSK3B, IL13, CDK6, JAK2
hsa04068	FoxO signaling pathway	5	8.56×10^{-3}	MAPK1, TGFBR1, NLK, CCNG2, BCL2L11
hsa05166	HTLV-I infection	6	1.86×10^{-2}	FOS, NRP1, ETS1, TGFBR1, GSK3B, SRF
MiR-101-5p				
hsa05200	Pathways in cancer	35	7.08×10^{-16}	XIAP, PTGS2, FOXO1, MMP1, TPM3, CCNE2, IGF1R, KRAS, CDKN2B, BCL2, SOS1, ITGAV, MYC, AKT3, PRKCA, BMP4, IL6, RALBP1, TGFBR1, CREBBP, *et al.*
hsa04068	FoxO signaling pathway	21	5.59×10^{-14}	IL6, SGK3, TGFBR1, CREBBP, SMAD4, SMAD3, FOXO1, SMAD2, MAPK10, IL7R, CCNG2, BCL2L11, ATM, IGF1R, NRAS, MAPK1, KRAS, CDKN2B, CCND2, SOS1, AKT3
hsa05161	Hepatitis B	20	2.82×10^{-12}	PRKCA, IL6, YWHAZ, TGFBR1, CREBBP, MAP2K4, CYCS, SMAD4, CDK6, MAPK10, STAT2, CCNE2, NRAS, MAPK1, KRAS, DDX3X, BCL2, NFATC2, MYC, AKT3
hsa04151	PI3K–Akt signaling pathway	27	7.91×10^{-11}	YWHAZ, RPS6KB1, IL7R, CCNE2, IGF1R, KRAS, SOS1, ITGAV, BCL2, ANGPT2, MYC, AKT3, GHR, PRKCA, IL6, FLT1, SGK3, MET, CDK6, BCL2L11, *et al.*
hsa04917	Prolactin signaling pathway	12	2.43×10^{-8}	MAPK1, NRAS, KRAS, TNFRSF11A, SOCS2, PRLR, CCND2, SOS1, ESR1, ESR2, MAPK10, AKT3
hsa04520	Adherens junction	12	2.43×10^{-8}	MAP3K7, MAPK1, IGF1R, TGFBR1, CREBBP, MET, SMAD4, SMAD3, SMAD2, WASL, YES1, CTNNA1
hsa05220	Chronic myeloid leukemia	12	2.83×10^{-8}	MAPK1, NRAS, KRAS, CRKL, HDAC2, TGFBR1, SOS1, SMAD4, CDK6, MYC, AKT3, PTPN11
hsa05205	Proteoglycans in cancer	18	3.80×10^{-8}	PRKCA, ERBB4, MET, ESR1, RPS6KB1, SDC2, FZD7, PTPN11, IGF1R, NRAS, MAPK1, KRAS, ITGAV, SOS1, MYC, FRS2, AKT3, TWIST1
hsa05210	Colorectal cancer	11	7.32×10^{-8}	MAPK1, KRAS, TGFBR1, BCL2, CYCS, SMAD4, SMAD3, SMAD2, MAPK10, MYC, AKT3
hsa04630	Jak–STAT signaling pathway	15	1.37×10^{-7}	IL6, SOCS2, IL6ST, LEPR, CREBBP, IL7R, STAT2, PTPN11, LEP, PRLR, CCND2, SOS1, MYC, AKT3, GHR

miR-101-3p was 78.0% (95% CI: 65.0–88.0%) and 79.0% (95% CI: 67.0–88.0%), respectively (Fig. 3A). In addition, the summary SROC of miR-101-3p was 0.86 (95% CI: 0.82–0.89; Fig. 3B). In addition, the PLR and NLR for HCC diagnosis were 3.803 (95% CI: 2.398–6.033) and 0.272 (95% CI: 0.169–0.439), respectively. Furthermore, the pre-test probability was 20 for miR-101-3p, and the corresponding positive and negative post-test probabilities of miR-101-3p were 49 and 6, respectively, suggesting that the power of miR-101-3p to diagnose real patients as HCC was 3.8 times the normal control (Fig. 4A). In addition, the likelihood ratio scattergram disclosed that the summary point of the PLR together with the NLR lies in the right lower quadrant (PLR < 10, NLR > 0.1; Fig. 4B).

With regard to miR-101-5p, a random effects model was also selected for further analysis (I^2 = 78.79% and 92.24%, for sensitivity and specificity, respectively, $P < 0.01$). The overall sensitivity and specificity were 79.0% (95% CI: 75.0–83.0%) and 60.0% (95% CI: 27.0–86.0%), respectively (Fig. 5A). The calculated AUC of the summary SROC was 0.80 (95% CI: 0.76–0.83; Fig. 5B). Additionally, the PLR was 1.981 (95% CI: 0.831–4.721), and the NLR was 0.349 (95% CI: 0.174–0.698); the pre-test probability of miR-101-5p was 20, and the corresponding positive and negative post-test probability of miR-101-5p was 33 and 8, respectively, suggesting that the power of miR-101-5p to diagnose real patients as HCC was 1.98 times the normal control (Fig. 6A). In addition, the summary point

Table 4. GO functional annotation for most significantly related targets of miR-101-3p.

GO ID	Term	Gene no.	*P*	Genes
BP				
GO: 0045944	Positive regulation of transcription from RNA polymerase II promoter	20	1.90×10^{-8}	CEBPA, SOX6, ZEB1, ZIC1, TET2, SOX9, PROX1, SRF, MYCN, PGR, MEF2D, FOS, ETS1, ZNF148, GSK3B, ASH1L, NEUROD1, TCF4, BCL9, SMARCA4
GO: 0045893	Positive regulation of transcription, DNA-templated	15	3.19×10^{-8}	KLF6, RSF1, TGFBR1, ARID1A, SOX9, ZIC1, PROX1, MYCN, MAPK1, FOS, ETS1, NEUROD1, PTCH1, TCF4, SMARCA4
GO: 0032355	Response to estradiol	6	4.40×10^{-5}	DUSP1, SOCS2, PTGS2, ETS1, EZH2, PTCH1
GO: 0008285	Negative regulation of cell proliferation	10	4.72×10^{-5}	CEBPA, PTGS2, ETS1, CDK6, JAK2, ZEB1, ARID2, PROX1, SRF, CDH5
GO: 0001764	Neuron migration	6	8.71×10^{-5}	NRP1, GJA1, PAFAH1B1, TOP2B, CXCL12, SRF
GO: 0001701	*In utero* embryonic development	7	1.49×10^{-4}	TGFBR1, MYO1E, GJA1, PTCH1, SOX6, SRF, BCL2L11
GO: 0000122	Negative regulation of transcription from RNA polymerase II promoter	12	2.32×10^{-4}	CUL3, CEBPA, JDP2, ZNF148, EZH2, PTCH1, ARID1A, SOX6, ZEB1, TCF4, PROX1, SMARCA4
GO: 0006366	Transcription from RNA polymerase II promoter	10	3.32×10^{-4}	CEBPA, MEF2D, FOS, ZNF148, ETS1, ASH1L, NEUROD1, ZIC1, SOX9, SRF
GO: 0018107	Peptidyl-threonine phosphorylation	4	5.73×10^{-4}	MAPK1, TGFBR1, GSK3B, NLK
GO: 0007179	Transforming growth factor beta receptor signaling pathway	5	6.53×10^{-4}	MAP3K7, FOS, TGFBR1, NLK, CDH5
CC				
GO: 0005654	Nucleoplasm	30	2.50×10^{-7}	ING3, RSF1, XPO5, XPO4, EZH2, ZEB1, SOX6, ZIC1, SOX9, SRF, ARID2, LARP1, CUL3, PGR, FOS, FBXW7, ZNF148, TOP2B, BCL9, NLK, *et al.*
GO: 0005634	Nucleus	40	1.24×10^{-5}	ING3, JDP2, RSF1, PTGS2, XPO5, EZH2, SOX6, ZEB1, SOX9, ZIC1, TIMP3, SRF, MAP3K7, CUL3, PGR, FOS, MSI1, SSX2IP, TOP2B, TCF4, *et al.*
GO: 0009897	External side of plasma membrane	6	1.54×10^{-3}	CLCN3, FGA, IL13, ABCA1, CXCL12, CDH5
GO: 0005901	Caveola	4	2.17×10^{-3}	MAPK1, PTGS2, PTCH1, JAK2
GO: 0009986	Cell surface	8	5.50×10^{-3}	CLCN3, NRP1, FGA, TGFBR1, CFTR, SPARC, CDH5, SLC7A11
GO: 0043234	Protein complex	7	5.73×10^{-3}	MAPK1, FBXW7, PTGS2, CFTR, SSX2IP, SOX9, SMARCA4
GO: 0000790	Nuclear chromatin	5	7.16×10^{-3}	EZH2, ARID1A, TCF4, SRF, SMARCA4
GO: 0005737	Cytoplasm	31	1.21×10^{-2}	ING3, PTGS2, XPO5, XPO4, EZH2, IL13, ZEB1, ZIC1, CCNG2, SRF, LIN28B, LARP1, MAP3K7, FBXW7, MSI1, TOP2B, ZMYM2, SOCS2, MYO1E, CFTR, *et al.*
GO: 0005769	Early endosome	5	1.28×10^{-2}	MAPK1, CLCN3, NRP1, GJA1, CFTR
GO: 0005794	Golgi apparatus	9	2.02×10^{-2}	CUL3, MAPK1, CLCN3, ZNF148, ASH1L, GJA1, PTCH1, ABCA1, BCL9
MF				
GO: 0005515	Protein binding	62	1.67×10^{-9}	JDP2, NRP1, RSF1, PTGS2, XPO5, XPO4, EZH2, IL13, GJA1, ZEB1, LARP1, MAP3K7, PGR, CUL3, FOS, ZNF148, SOCS2, CFTR, ARID1A, CDK6, *et al.*
GO: 0000978	RNA polymerase II core promoter proximal region sequence-specific DNA binding	11	2.20×10^{-6}	PGR, CEBPA, MEF2D, FOS, JDP2, ZNF148, NEUROD1, TCF4, ZIC1, SRF, SMARCA4
GO: 0001077	Transcriptional activator activity, RNA polymerase II core promoter proximal region sequence-specific binding	9	6.46×10^{-6}	PGR, CEBPA, MEF2D, FOS, NEUROD1, TCF4, ZIC1, SOX9, SRF
GO: 0008134	Transcription factor binding	9	2.47×10^{-5}	CEBPA, MAPK1, FOS, ETS1, NLK, NEUROD1, ZEB1, SRF, SMARCA4

Table 4. (Continued).

GO ID	Term	Gene no.	*P*	Genes
GO: 0003700	Transcription factor activity, sequence-specific DNA binding	15	3.92×10^{-5}	CEBPA, JDP2, SOX6, ZEB1, SOX9, ZIC1, PROX1, SRF, MYCN, PGR, MEF2D, FOS, ETS1, NEUROD1, TCF4
GO: 0003677	DNA binding	20	4.29×10^{-5}	CEBPA, KLF6, ZMYM2, EZH2, ARID1A, SOX6, ZEB1, TET2, ARID2, LIN28B, PROX1, MYCN, PGR, MAPK1, FOS, SP2, ETS1, ASH1L, TOP2B, TCF4
GO: 0030332	Cyclin binding	4	7.72×10^{-5}	CUL3, FBXW7, PTCH1, CDK6
GO: 0046982	Protein heterodimerization activity	10	1.38×10^{-4}	CUL3, MEF2D, FOS, CLCN3, JDP2, NEUROD1, SOX6, TOP2B, TCF4, SOX9
GO: 0003682	Chromatin binding	9	2.29×10^{-4}	FOS, JDP2, EZH2, ASH1L, NEUROD1, ZEB1, TOP2B, TCF4, SOX9
GO: 0005102	Receptor binding	8	6.95×10^{-4}	PGR, FGA, CADM2, GJA1, JAK2, ABCA1, CXCL12, CDH5

of the PLR combined with the NLR also lies in the right lower quadrant (PLR < 10, NLR > 0.1), which was consistent with the Fagan's nomogram result (Fig. 6B).

Publication bias

Publication bias was conducted by using the Deeks' funnel plot asymmetry test. According to the results, the funnel plots that represented every study were almost symmetric, suggesting that publication bias from the studies included was absent in our study. The obtained *P*-values of 0.718 and 0.447 for miR-101-3p and miR-101-5p, respectively, also revealed the absence of publication bias (Fig. 7).

Bioinformatic analysis

To improve understanding of the function of miR-101, the potential target genes of miR-101-3p and miR-101-5p in HCC were identified separately. Based on the prediction software and NLP, 73 target genes corresponding to miR-101-3p and 90 target genes corresponding to miR-101-5p were obtained. Subsequently, bioinformatic analyses were conducted to investigate the function and pathways of target genes of miR-101 associated with HCC. All of the target genes were inputted into DAVID for bioinformatic analysis.

KEGG pathway enrichment analysis

Our study revealed that 23 KEGG pathways corresponding to miR-101-3p were enriched, from which the top five pathways in which target genes were enriched were (a) the adherens junction pathway (hsa04520: $P = 8.53 \times 10^{-4}$), (b) the leishmaniasis pathway (hsa05140: $P = 8.53 \times 10^{-4}$), (c) the prolactin signaling pathway (hsa04917: $P = 8.53 \times 10^{-4}$), (d) pathways in cancer (hsa05200: $P = 0.002$) and (e) the mitogen-activated protein kinase (MAPK) signaling pathway (hsa04010: $P = 0.004$). For miR-101-5p, 90 KEGG pathways were enriched, and the top pathways were (a) pathways in cancer (hsa05200: $P = 7.08 \times 10^{-16}$), (b) the forkhead box O (FoxO) signaling pathway (hsa04068: $P = 5.59 \times 10^{-14}$), (c) hepatitis B (hsa05161: $P = 2.82 \times 10^{-12}$), (d) the phosphoinositide-3-kinase (PI3K)–Akt signaling pathway (hsa04151: $P = 7.91 \times 10^{-11}$) and (e) the prolactin signaling pathway (hsa04917: $P = 2.43 \times 10^{-8}$). The top 30 pathways associated with miR-101-3p and miR-101-5p are shown in Figs 8 and 9, respectively, and all of the pathways are displayed in Table 3.

GO enrichment analysis

As shown in Tables 4 and 5, the GO enrichment was composed of the BP, CC and MF categories. In the BP category for miR-101-3p, we can observe that the 73 target genes were mainly enriched in (a) positive regulation of transcription from the RNA polymeraseIIpromoter (GO: 0045944, $P = 1.90 \times 10^{-8}$), (b) positive regulation of transcription, DNA-templated (GO: 0045893, $P = 3.19 \times 10^{-8}$) and (c) response to estradiol (GO: 0032355, $P = 4.40 \times 10^{-5}$). In addition, in the CC category, (a) nucleoplasm (GO: 0005654, $P = 2.50 \times 10^{-7}$), (b) nucleus (GO: 0005634, $P = 1.24 \times 10^{-5}$) and (c) external side of plasma membrane (GO: 0009897, $P = 0.002$) remained the top three enriched items. With regard to MF, the top ranking three items were protein binding (GO: 0005515, $P = 1.67 \times 10^{-9}$), RNA polymerase II core promoter proximal region sequence-specific DNA binding (GO: 0000978, $P = 2.20 \times 10^{-6}$) and transcriptional activator activity, RNA polymerase II core

Table 5. GO functional annotation for most significantly related targets of miR-101-5p.

GO ID	Term	Gene no.	*P*	Genes
BP				
GO: 0043066	Negative regulation of apoptotic process	29	2.01×10^{-13}	YWHAZ, MTDH, ERBB4, XIAP, IL6ST, FOXO1, PRKDC, RPS6KB1, IGF1R, DDX3X, BCL2, TPT1, GLO1, MYC, TWIST1, BMP4, IL6, TBX3, SOCS2, SMAD3, *et al.*
GO: 0045893	Positive regulation of transcription, DNA-templated	28	2.34×10^{-11}	RSF1, ERBB4, FOXO1, ZIC1, ASPH, NFATC2, MYC, BMP4, KLF6, IL6, TBX3, TGFBR1, CREBBP, SMAD5, SMAD4, ESR1, ATAD2, SMAD3, SMAD2, ESR2, *et al.*
GO: 0045944	Positive regulation of transcription from RNA polymerase II promoter	38	5.43×10^{-11}	PRKDC, FOXO1, ZEB2, NR3C1, SOX6, ZEB1, ZIC1, PGR, IL17A, BARX2, CDKN2B, DDX3X, ZNF148, NFATC2, YES1, MYC, TWIST1, CKAP2, BMP4, IL6,*et al.*
GO: 0000122	Negative regulation of transcription from RNA polymerase II promoter	32	9.99×10^{-11}	JDP2, MTDH, USP2, FOXO1, ZEB2, SOX6, ZEB1, BARX2, ZNF148, NFATC2, MYC, TWIST1, BMP4, DAB2IP, TBX3, YY1, CREBBP, SMAD4, ESR1, KLF17, *et al.*
GO: 0008284	Positive regulation of cell proliferation	25	4.77×10^{-10}	ERBB4, IL6ST, IGF1R, CD47, KRAS, TNFRSF11A, ITGAV, BCL2, MYC, IL6, FLT1, KLB, TBX3, TGFBR1, PROX1, TET1, LEP, MAPK1, HDAC2, CRKL, *et al.*
GO: 0043065	Positive regulation of apoptotic process	19	7.80×10^{-9}	BMP4, IL6, DAB2IP, ERBB4, PTGS2, PRKDC, FOXO1, FRZB, LATS1, BCL2L11, ATM, BAK1, TRIM35, ITGA6, DDX3X, SFRP1, ATG7, SOS1, UNC5C
GO: 0050900	Leukocyte migration	12	1.23×10^{-7}	NRAS, CD47, KRAS, ITGA6, ITGAV, SOS1, TREM1, YES1, ANGPT2, MMP1, SLC7A11, PTPN11
GO: 0008285	Negative regulation of cell proliferation	18	2.36×10^{-6}	BMP4, IL6, DAB2IP, ERBB4, PTGS2, SMAD4, SMAD2, CDK6, ZEB1, FRZB, ARID2, PROX1, SLIT3, BAK1, SPRY1, CDKN2B, SFRP1, MDM4
GO: 0001568	Blood vessel development	7	3.73×10^{-6}	MIB1, LAMA4, CRKL, TBX3, ITGAV, FOXO1, AHR
GO: 0071498	Cellular response to fluid shear stress	5	7.02×10^{-6}	MTSS1, PTGS2, CA2, NFE2L2, TFPI2
CC				
GO: 0005829	Cytosol	67	3.59×10^{-8}	RPL36A, FOXO1, RPS6KB1, LATS1, MAP3K7, CCNE2, BAK1, SPRY1, GSTM3, CDKN2B, MAT1A, ATG7, MYC, PRKCA, DAB2IP, SOCS2, SGK3, RALBP1, G3BP1, CYCS, *et al.*
GO: 0005654	Nucleoplasm	53	1.23×10^{-5}	RSF1, XPO4, FOXO1, RPS6KB1, ZEB1, ZIC1, PGR, CCNE2, SPRY1, CDKN2B, ZNF148, MYC, AKT3, PRKCA, DTL, ESR1, CDK6, ESR2, AHR, MCM6, *et al.*
GO: 0009897	External side of plasma membrane	12	1.50×10^{-5}	EPHA5, VCAM1, CLCN3, IL17A, IL6, TNFRSF11A, ITGA6, CD40LG, IL6ST, ITGAV, CD274, IL7R
GO: 0005634	Nucleus	84	2.85×10^{-5}	JDP2, RSF1, PTGS2, CPEB4, FOXO1, ZEB2, RPS6KB1, ZEB1, ZIC1, MAP3K7, CCNE2, PGR, GSTM3, BARX2, CDKN2B, TPT1, LOX, TFPI2, MYC, ANGPT2, *et al.*
GO: 0005737	Cytoplasm	81	4.65×10^{-5}	MTSS1, PTGS2, XPO4, CPEB4, FOXO1, RPS6KB1, ZEB1, ZIC1, MAP3K7, SPRY1, GSTM3, CDKN2B, ATG7, TPT1, FRS2, AKT3, PRKCA, DAB2IP, SOCS2, LPGAT1, *et al.*
GO: 0071141	SMAD protein complex	4	6.01×10^{-5}	SMAD5, SMAD4, SMAD3, SMAD2
GO: 0005667	Transcription factor complex	10	1.97×10^{-4}	BARX2, YY1, SMAD5, SMAD4, SMAD3, PRKDC, SMAD2, DACH1, ZEB1, AHR
GO: 0043235	Receptor complex	8	3.74×10^{-4}	IGF1R, FLT1, ERBB4, LEPR, TGFBR1, NTRK2, SMAD3, GHR
GO: 0009986	Cell surface	16	5.76×10^{-4}	CLCN3, TGFBR1, MET, RPS6KB1, CFTR, SDC2, SLC7A11, VCAM1, ITGA6, SULF2, PRLR, SFRP1, CD40LG, ITGAV, CNTN2, GHR
GO: 0005622	Intracellular	27	1.45×10^{-3}	PRKCA, KLB, TGFBR1, G3BP1, SMAD5, SOCS6, SMAD4, DCDC2, SMAD3, MAPK10, LATS1, SEC63, WSB1, MAPK1, RND3, NRAS, TRIM35, KRAS, SFRP1, TRIM33, *et al.*

Table 5. (Continued).

GO ID	Term	Gene no.	*P*	Genes
MF				
GO: 0005515	Protein binding	147	5.59×10^{-14}	MTSS1, RPL36A, JDP2, PTGS2, IL6ST, XPO4, FOXO1, RPS6KB1, PGR, MAP3K7, CD47, BAK1, CDKN2B, ATG7, TPT1, ASPH, LOX, FRS2, TWIST1, DAB2IP, *et al.*
GO: 0008134	Transcription factor binding	18	1.69×10^{-8}	YWHAZ, CREBBP, ESR1, SMAD3, PRKDC, SMAD2, ZEB1, AHR, MAPK1, HDAC2, SP1, DDX3X, PSMD10, ATG7, BCL2, NFATC2, MYC, TWIST1
GO: 0001078	Transcriptional repressor activity, RNA polymerase II core promoter proximal region sequence-specific binding	10	3.79×10^{-6}	JDP2, TBX3, ZNF148, YY1, CREBBP, KLF17, FOXO1, DACH1, NFATC2, PROX1
GO: 0005524	ATP binding	37	5.87×10^{-6}	CLCN3, ERBB4, PFKFB2, STK17B, PRKDC, RPS6KB1, LATS1, MAP3K7, IGF1R, KRAS, DDX3X, MAT1A, HSPE1, YES1, AKT3, PRKCA, FLT1, SGK3, TGFBR1, UBE4B, *et al.*
GO: 0000978	RNA polymerase II core promoter proximal region sequence-specific DNA binding	15	4.05×10^{-5}	JDP2, TBX3, SMAD4, ESR1, KLF17, SMAD3, SMAD2, NR3C1, ZIC1, PGR, HDAC2, SP1, ZNF148, NFATC2, MYC
GO: 0042802	Identical protein binding	22	8.15×10^{-5}	MTSS1, YWHAZ, DAB2IP, XIAP, USP2, SMAD4, ESR1, SMAD3, CLDN10, RPS6KB1, STAT2, MCM6, PBLD, IGF1R, BAK1, MAPK1, GLUL, GSTM3, SFRP1, BCL2, CNTN2, GBP1
GO: 0008270	Zinc ion binding	29	8.19×10^{-5}	RSF1, XIAP, NR3C1, ZEB1, LIN28B, MMP1, PGR, GLO1, XAF1, RCHY1, PRKCA, ZMYM2, YY1, CREBBP, ESR1, SMAD3, WHSC1, ESR2, TET2, TET1, *et al.*
GO: 0004672	Protein kinase activity	14	1.79×10^{-4}	PRKCA, SGK3, TGFBR1, MET, MAP2K4, STK17B, PRKDC, RPS6KB1, PBK, MAPK10, MAP3K7, MAP4K4, HIPK2, AKT3
GO: 0043565	Sequence-specific DNA binding	17	2.04×10^{-4}	JDP2, TBX3, SMAD4, ESR1, SMAD3, FOXO1, WHSC1, NR3C1, ESR2, SOX6, PGR, HDAC2, SP1, ZNF148, BCL2, NFE2L2, MYC
GO: 0019899	Enzyme binding	13	3.32×10^{-4}	PRKCA, PTGS2, UBE4B, ESR1, PRKDC, CFTR, ESR2, PGR, GSTM3, HDAC2, MDM4, YES1, GBP1

promoter proximal region sequence-specific binding (GO: 0001077, $P = 6.46 \times 10^{-6}$). In the same way, the top three enriched pathways of the 119 target genes of miR-101-5p in the BP category were (a) negative regulation of the apoptotic process (GO: 0043066, $P = 2.01 \times 10^{-13}$), (b) positive regulation of transcription, DNA-templated, negative regulation of transcription from the RNA polymerase II promoter (GO: 0045893, $P = 2.34 \times 10^{-11}$) and (c) positive regulation of transcription from the RNA polymerase II promoter (GO: 0045944, $P = 5.43 \times 10^{-11}$). For the CC category, (a) cytosol (GO: 0005829, $P = 3.59 \times 10^{-8}$), (b) nucleoplasm (GO: 0005654, $P = 1.23 \times 10^{-5}$) and (c) external side of the plasma membrane (GO: 0009897, $P = 1.50 \times 10^{-5}$) were the most enriched terms. In addition, in the MF category, the utmost significant three items were (a) protein binding (GO: 0005515, $P = 5.59 \times 10^{-14}$), (b) transcription factor binding (GO: 0008131, $P = 1.69 \times 10^{-8}$) and (c) transcriptional repressor activity, RNA polymerase II core promoter proximal region sequence-specific binding (GO: 0001078. $P = 3.79 \times 10^{-6}$). All of the GO enrichment items are visualized in the GO network (Figs 10 and 11).

Protein–protein interaction network

A PPI network was designed to screen out the hub genes according to the degree to which each of the genes appeared in the network. Here, the PPI network was constructed by using the STRING database. As shown in Figs 12 and 13, *FOX*, *SMARCA4* and *MAPK1* remained the top three utmost important genes for miR-101-3p, while *ESR1*, *KRAS*, *NRAS*, *FOXO1*, *CREBBP* and *SMAD3* were regarded as the hub genes for miR-101-5p.

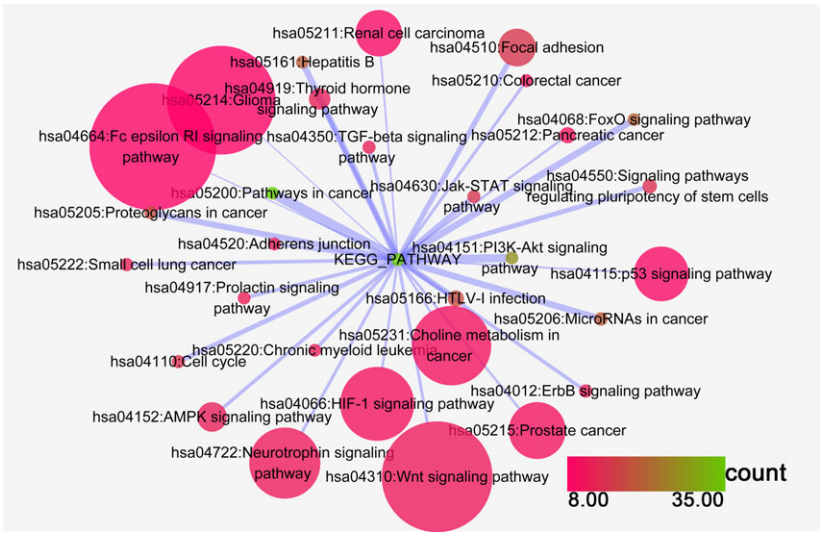

Fig. 10. GO functional analysis of miR-101-3p in HCC. Top 10 terms of each category are displayed, and every node represents different BP terms; the map node size represents the *P* value of targets, low values are indicated by large nodes, and the node color represents the gene count number with low values indicated by pink.

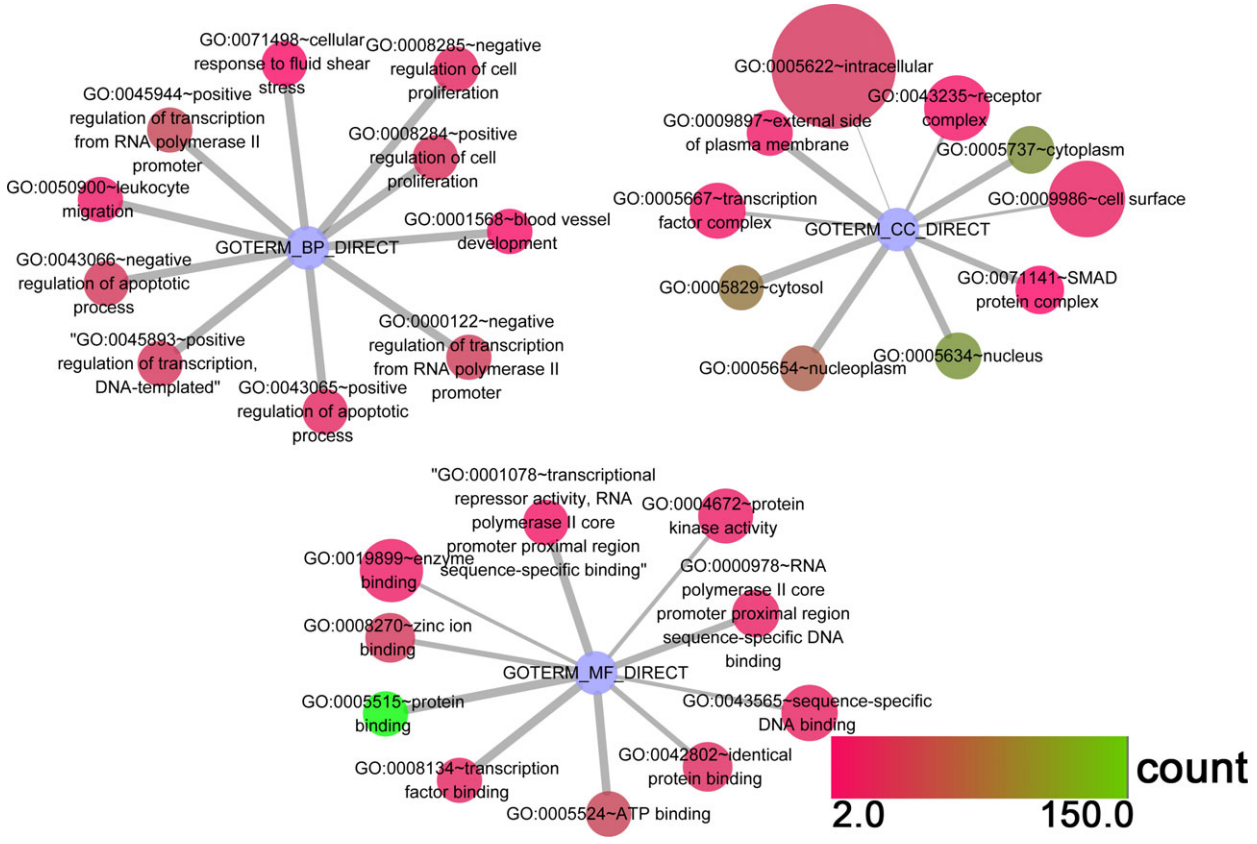

Fig. 11. GO functional analysis of miR-101-5p in HCC. Top 10 terms of each category are displayed, and every node represents different BP terms; the map node size represents the *P* value of targets, low values are indicated by large nodes, and the node color represents the gene count number with low values indicated by pink.

Discussion

In the present study, we investigated the relationship between miR-101 expression and clinicopathological parameters. TCGA data showed that the miR-101 level was significantly lower in HCC than in para-non-cancerous liver tissues, and great diagnostic value of miR-101 in HCC was found. Additionally,

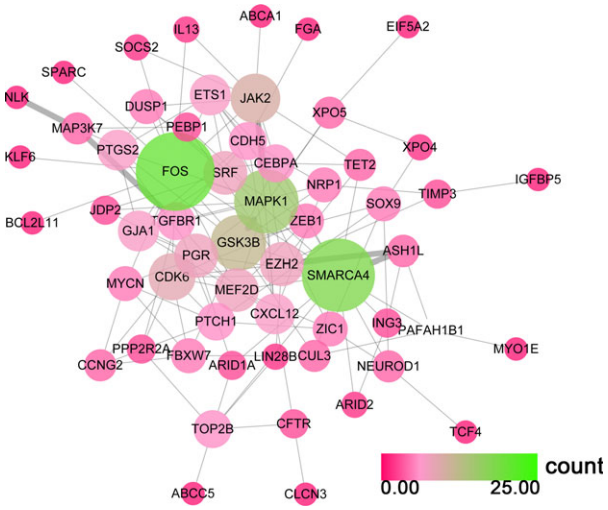

Fig. 12. The PPI network of miR-101-3p potential targets. Both the color and the size of the nodes reflect the connectivity degrees of two nodes; nodes with a green color are perceived as hub genes.

miR-101 was negatively correlated with pathological stage, pathological T stage and histological grade. Since these clinicopathological parameters are indicators of tumor deterioration and progression, monitoring the level of miR-101 may have a certain significance in the progression of HCC.

Accumulating studies have indicated that dysregulation of circulating miRNAs could be a biomarker of tumorigenesis, development and invasion in various cancers including prostate cancer, gastric cancer, ovarian cancer, breast cancer and lung cancer [30,46–49]. A diagnostic value for circulating miR-101-3p/5p in HCC has also been reported [50,51]. Both of these studies validated that a lower miR-101-3p/5p level had diagnostic potential for HCC. However, due to the limited number of available publications, the exact diagnostic value of miR-101 and the difference between miR-101-3p and miR-101-5p are still unclear. Alpha-fetoprotein (AFP), as the traditional marker of liver diseases, has been used for HCC diagnosis in the clinic. Recently, He *et al.* [33] conducted a meta-analysis with 10 data sets (879 HCC patients and 1028 controls) assessing AFP for HCC diagnosis and revealed that the AUC–SROC of pooled AFP was 0.82 (95% CI: 0.78–0.85), with sensitivity of 0.631 (95% CI: 0.552–0.703) and specificity of 0.943 (95% CI: 0.875–0.975). Here, we first combined gene expression microarray datasets from the GEO database and RNA-seq from TCGA database, as well as two studies, to further confirm the diagnostic efficacy of miR-101-3p and miR-101-5p and then discover the difference between the two mature mRNAs. Our findings suggested that the pooled diagnostic accuracy of miR-101-3p for HCC (SROC: 0.86 (95% CI: 0.82–0.89); sensitivity and specificity were 78.0% (95% CI: 65.0–88.0%) and 79.0% (95% CI: 0.67–88.0%), respectively), which showed a slightly higher diagnostic value than AFP. As for miR-101-5p, the SROC was 0.80 (95% CI: 0.76–0.83), a little bit lower than AFP, but it also showed a moderate value for HCC diagnosis, which is comparable to AFP's diagnostic value.

Even though miR-101-3p/5p expression showed a high diagnostic value for HCC, the heterogeneity among the studies must be considered. Since our study indicated that heterogeneity from the threshold effect was absent, we deduced that the heterogeneity may be caused by the different data platforms and the large gaps between each study. Considering that the number of studies was small, we did not conduct a subgroup analysis.

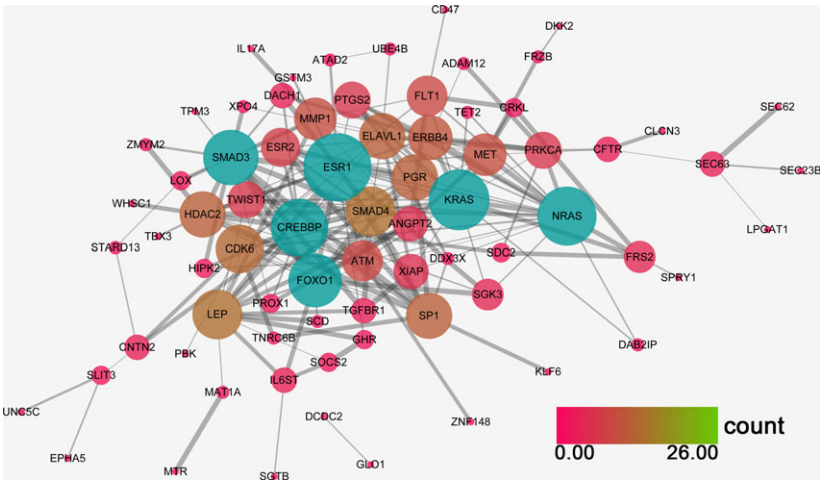

Fig. 13. The PPI network of miR-101-5p potential targets. Both the color and the size of the nodes reflect the connectivity degrees of two nodes; nodes with a blue color are perceived as hub nodes.

Subsequently, bioinformatic analysis was performed to determine the molecular mechanism of miR-101-3p/5p in HCC. In the past, researchers exploring the molecular mechanism of miRNAs only concentrated on one or two target genes. For example, Varambally *et al.* [52] first reported that *EZH2* was the target gene of miR-101 (3p and 5p were not distinguished) several years ago. Another study confirmed that miR-101 (3p and 5p were not distinguished) inhibits HCC progression and metastasis through *EZH2* down-regulation [53]. Liu *et al.* [54] identified another target gene of miR 101 (3p and 5p were not distinguished), *VEGF C*, which promotes invasion and migration. *MCL-1* and *COX-2*, which play a role in tumorigenesis, have also been identified as the target genes of miR-101 (3p and 5p were not distinguished) [31,55]. In addition, metastasis of HCC has been shown to be affected by different target genes of miR-101 (3p and 5p were not distinguished), such as *STMN1* [56] and *PTEN* [57]. Since a single miRNA can target multiple genes to achieve its biological and clinical functions, the exploration of the relevant gene network can reveal the widespread molecular mechanism of miR-101-3p/5p. Hence, we identified potential target genes of miR-101-3p/5p *in silico*. Moreover, we further narrowed the list by analyzing the genes that overlapped with the differentially expressed genes of HCC identified via NLP. Next, these target genes were subjected to KEGG pathway annotation and GO enrichment analysis by using the DAVID. The target genes of both miR-101-3p and miR-101-5p are involved in pathways in cancer, hepatitis B and the MAPK signaling pathway. These results reveal that miR-101 probably contributes to the tumorigenesis and metastasis of HCC. Previous studies have reported the role of these pathways in liver cancer [58,59]. The GO term analysis indicated that these potential target genes of miR-101-3p/5p were significantly involved in the regulation of the cell cycle and cell proliferation, which are associated with tumor occurrence or stepwise development.

Furthermore, we constructed the PPI network with potential target genes, showing that miR-101-3p probably targets *FOS*, *SMARCA4*, *MAPK1*, *GSK3B* and *JAK2* to exert its function in HCC. Li *et al.* [60] reported that *FOS* acts as a regulator of cell proliferation, differentiation and transformation, and miR-101 inhibits cell invasion and migration via down-regulation of *FOS*. MAPK1 has also been reported to be involved in a variety of cellular processes, such as differentiation, proliferation and development through the MAPK pathway [61]. JAK2 is a protein tyrosine kinase, and recent evidence has demonstrated that miR-101 (3p and 5p were not distinguished) inhibits breast cancer cell proliferation and promotes apoptosis by targeting JAK2 [49]. Previous studies reveal that miR-101-3p might regulate the occurrence and development of HCC by targeting various genes, and tumorigenesis probably results from the abnormality of multiple genes. Of course, the correlation of those potential key genes of miR-101-3p needs further experimental validation. Next, a functional analysis of these target genes *in vitro* and *in vivo* will need to be conducted, such as by RNA interference and cellular transfection, luciferase reporter assay, western blot and so on. miR-101-5p possibly targets *ESR1*, *KRAS*, *CREBBP*, *FOXO1* and *SMAD3* through different pathways. Among them, *KRAS*, a Kirsten ras oncogene homolog, was reported to have functional synergy with HBx in HCC initiation and progression [62], and *FOXO1* has been proposed to inhibit EMT transcriptional activators in HCC [63,64]. Additionally, Hishida *et al.* [65] indicated that *ESR1* is a tumor suppressor gene in HCC. Taken together, the hub genes identified may perform key roles in HCC. Further investigation appears to be necessary to confirm their exact function in HCC.

Taken together, the present study validated the down-regulation of the two opposing strands, miR-101-3p and miR-101-5p, in HCC clinical specimens; however, miR-101-3p held a greater value for HCC diagnosis. Bioinformatic analysis revealed that miR-101-3p and miR-101-5p are involved in the same or similar signaling pathways through regulating a different set of target genes. The fact that miR-101-3p and miR-101-5p are involved in these signaling pathways suggests that the expression of miR-101-3p and miR-101-5p is close in HCC tissues, and they may function cooperatively with each other in the differentiation, proliferation and development of HCC.

In conclusion, we provide a comprehensive analysis of miR-101-3p/5p and evaluated the value of miR-101-3p and miR-101-5p as biomarkers for the early diagnosis of HCC. In addition, we investigated the prospective molecular mechanisms of these two opposing strands *in silico*. Our results provide a deeper understanding of the role of miR-101-3p/5p in HCC and facilitate the possible development of a miRNA-based targeted therapy of HCC. However, several limitations should be considered in this study. First, the total number of studies included was limited; second, further experiments *in vitro* and *in vivo* are still required to confirm the function of the target genes.

Acknowledgements

The study was supported by the Fund of Youth Science Foundation of Guangxi Medical University

(GXMUYSF201624). The funder had no role in study design, data collection and analysis, decision to publish, or preparation of the manuscript.

Author contributions

XY and Y-YP contributed equally in this study. XY, Y-YP and PL collected data and wrote the paper draft; R-QH and J-MC contributed to the analysis; JM, GC and HY designed the study, supervised the report and corrected the manuscript.

References

1 Siegel RL, Miller KD and Jemal A (2017) Cancer statistics, 2017. *CA Cancer J Clin* **67**, 7–30.
2 Sherman M (2010) Hepatocellular carcinoma: epidemiology, surveillance, and diagnosis. *Semin Liver Dis* **30**, 3–16.
3 Xie Y, Yao Q, Butt AM, Guo J, Tian Z, Bao X, Li H, Meng Q and Lu J (2014) Expression profiling of serum microRNA-101 in HBV-associated chronic hepatitis, liver cirrhosis, and hepatocellular carcinoma. *Cancer Biol Ther* **15**, 1248–1255.
4 Calin GA and Croce CM (2006) MicroRNA signatures in human cancers. *Nat Rev Cancer* **6**, 857–866.
5 Bartel DP (2004) MicroRNAs: genomics, biogenesis, mechanism, and function. *Cell* **116**, 281–297.
6 Harfe BD (2005) MicroRNAs in vertebrate development. *Curr Opin Genet Dev* **15**, 410–415.
7 Jiang J, Gusev Y, Aderca I, Mettler TA, Nagorney DM, Brackett DJ, Roberts LR and Schmittgen TD (2008) Association of microRNA expression in hepatocellular carcinomas with hepatitis infection, cirrhosis, and patient survival. *Clin Cancer Res* **14**, 419–427.
8 Fu Y, Wei X, Tang C, Li J, Liu R, Shen A and Wu Z (2013) Circulating microRNA-101 as a potential biomarker for hepatitis B virus-related hepatocellular carcinoma. *Oncol Lett* **6**, 1811–1815.
9 Liao Q, Han P, Huang Y, Wu Z, Chen Q, Li S, Ye J and Wu X (2015) Potential role of circulating microRNA-21 for hepatocellular carcinoma diagnosis: a meta-analysis. *PLoS ONE* **10**, e0130677.
10 Hou C, Tan G and Feng S (2014) Clinical significance of microRNA expressions in diagnosing uterine cancer and predicting lymph node metastasis. *Tumour Biol* **35**, 10789–10798.
11 Wang H, Wu S, Zhao L, Zhao J, Liu J and Wang Z (2015) Clinical use of microRNAs as potential non-invasive biomarkers for detecting non-small cell lung cancer: a meta-analysis. *Respirology* **20**, 56–65.
12 Wang N, Chen P, Huang LP and Wang TZ (2016) Prognostic significance of microRNA-10b overexpression in breast cancer: a meta-analysis. *Genet Mol Res* **15**, gmr.15027350. https://doi.org/10.4238/gmr.15027350
13 Slattery ML, Herrick JS, Pellatt DF, Mullany LE, Stevens JR, Wolff E, Hoffman MD, Wolff RK and Samowitz W (2016) Site-specific associations between miRNA expression and survival in colorectal cancer cases. *Oncotarget* **7**, 60193–60205.
14 Xu P, Zhu Y, Sun B and Xiao Z (2016) Colorectal cancer characterization and therapeutic target prediction based on microRNA expression profile. *Sci Rep* **6**, 20616.
15 Tang S, Wu WK, Li X, Wong SH, Wong N, Chan MT, Sung JJ and Yu J (2016) Stratification of digestive cancers with different pathological features and survival outcomes by MicroRNA expression. *Sci Rep* **6**, 24466.
16 Mott JL (2009) MicroRNAs involved in tumor suppressor and oncogene pathways: implications for hepatobiliary neoplasia. *Hepatology* **50**, 630–637.
17 Visone R, Petrocca F and Croce CM (2008) MicroRNAs in gastrointestinal and liver disease. *Gastroenterology* **135**, 1866–1869.
18 Almeida MI, Reis RM and Calin GA (2011) MicroRNA history: discovery, recent applications, and next frontiers. *Mutat Res* **717**, 1–8.
19 Almeida MI, Nicoloso MS, Zeng L, Ivan C, Spizzo R, Gafa R, Xiao L, Zhang X, Vannini I, Fanini F *et al.* (2012) Strand-specific miR-28-5p and miR-28-3p have distinct effects in colorectal cancer cells. *Gastroenterology* **142**, 886–896.e9.
20 Gong J, Wu Y, Zhang X, Liao Y, Sibanda VL, Liu W and Guo AY (2014) Comprehensive analysis of human small RNA sequencing data provides insights into expression profiles and miRNA editing. *RNA Biol* **11**, 1375–1385.
21 Yan F, Shen N, Pang J, Xie D, Deng B, Molina JR, Yang P and Liu S (2014) Restoration of miR-101 suppresses lung tumorigenesis through inhibition of DNMT3a-dependent DNA methylation. *Cell Death Dis* **5**, e1413.
22 Yao YL, Ma J, Wang P, Xue YX, Li Z, Zhao LN, Li ZQ, Feng TD and Liu YH (2015) miR-101 acts as a tumor suppressor by targeting Kruppel-like factor 6 in glioblastoma stem cells. *CNS Neurosci Ther* **21**, 40–51.
23 Wei X, Tang C, Lu X, Liu R, Zhou M, He D, Zheng D, Sun C and Wu Z (2015) MiR-101 targets DUSP1 to regulate the TGF-beta secretion in sorafenib inhibits macrophage-induced growth of hepatocarcinoma. *Oncotarget* **6**, 18389–18405.
24 Zhou X, Xia Y, Li L, and Zhang G (2015) MiR-101 inhibits cell growth and tumorigenesis of *Helicobacter pylori* related gastric cancer by repression of SOCS2. *Cancer Biol Ther* **16**, 160–169.

25 Ye Z, Yin S, Su Z, Bai M, Zhang H, Hei Z and Cai S (2016) Downregulation of miR-101 contributes to epithelial-mesenchymal transition in cisplatin resistance of NSCLC cells by targeting ROCK2. *Oncotarget* **7**, 37524–37535.
26 Hou J, Lin L, Zhou W, Wang Z, Ding G, Dong Q, Qin L, Wu X, Zheng Y, Yang Y *et al.* (2011) Identification of miRNomes in human liver and hepatocellular carcinoma reveals miR-199a/b-3p as therapeutic target for hepatocellular carcinoma. *Cancer Cell* **19**, 232–243.
27 Wei X, Xiang T, Ren G, Tan C, Liu R, Xu X and Wu Z (2013) miR-101 is down-regulated by the hepatitis B virus x protein and induces aberrant DNA methylation by targeting DNA methyltransferase 3A. *Cell Signal* **25**, 439–446.
28 Zhang Y, Guo X, Xiong L, Kong X, Xu Y, Liu C, Zou L, Li Z, Zhao J and Lin N (2012) MicroRNA-101 suppresses SOX9-dependent tumorigenicity and promotes favorable prognosis of human hepatocellular carcinoma. *FEBS Lett* **586**, 4362–4370.
29 Sheng Y, Li J, Zou C, Wang S, Cao Y, Zhang J, Huang A and Tang H (2014) Downregulation of miR-101-3p by hepatitis B virus promotes proliferation and migration of hepatocellular carcinoma cells by targeting Rab5a. *Arch Virol* **159**, 2397–2410.
30 Wang HJ, Ruan HJ, He XJ, Ma YY, Jiang XT, Xia YJ, Ye ZY and Tao HQ (2010) MicroRNA-101 is down-regulated in gastric cancer and involved in cell migration and invasion. *Eur J Cancer* **46**, 2295–2303.
31 Su H, Yang JR, Xu T, Huang J, Xu L, Yuan Y and Zhuang SM (2009) MicroRNA-101, down-regulated in hepatocellular carcinoma, promotes apoptosis and suppresses tumorigenicity. *Cancer Res* **69**, 1135–1142.
32 Liu N, Zhang L, Wang Z, Cheng Y, Zhang P, Wang X, Wen W, Yang H, Liu H, Jin W *et al.* (2017) MicroRNA-101 inhibits proliferation, migration and invasion of human glioblastoma by targeting SOX9. *Oncotarget* **8**, 19244–19254.
33 He S, Hu XW, Wang D, Han LF, Zhang DC and Wei C (2016) Accuracy of microRNAs for the diagnosis of hepatocellular carcinoma: a systematic review and meta-analysis. *Clin Res Hepatol Gastroenterol* **40**, 405–417.
34 Ha SY, Kim JH, Yang JW, Bae H, Cho HY and Park CK (2016) Expression of DBC1 is associated with poor prognosis in hepatitis virus-related hepatocellular carcinoma. *Pathol Res Pract* **212**, 616–621.
35 Kindrat I, Tryndyak V, de Conti A, Shpyleva S, Mudalige TK, Kobets T, Erstenyuk AM, Beland FA and Pogribny IP (2016) MicroRNA-152-mediated dysregulation of hepatic transferrin receptor 1 in liver carcinogenesis. *Oncotarget* **7**, 1276–1287.
36 Jin H, Yu M, Lin Y, Hou B, Wu Z, Li Z and Sun J (2016) MiR-502-3P suppresses cell proliferation, migration, and invasion in hepatocellular carcinoma by targeting SET. *Onco Targets Ther* **9**, 3281–3289.
37 Mourelatos Z, Dostie J, Paushkin S, Sharma A, Charroux B, Abel L, Rappsilber J, Mann M and Dreyfuss G (2002) miRNPs: a novel class of ribonucleoproteins containing numerous microRNAs. *Genes Dev* **16**, 720–728.
38 Chen L and Jin H (2014) MicroRNAs as novel biomarkers in the diagnosis of non-small cell lung cancer: a meta-analysis based on 20 studies. *Tumour Biol* **35**, 9119–9129.
39 Higgins JP and Thompson SG (2002) Quantifying heterogeneity in a meta-analysis. *Stat Med* **21**, 1539–1558.
40 Dweep H and Gretz N (2015) miRWalk2.0: a comprehensive atlas of microRNA-target interactions. *Nat Methods* **12**, 697.
41 Chang EK, Yu CY, Clarke R, Hackbarth A, Sanders T, Esrailian E, Hommes DW and Runyon BA (2016) Defining a patient population with cirrhosis: an automated algorithm with natural language processing. *J Clin Gastroenterol* **50**, 889–894.
42 Alsawas M, Alahdab F, Asi N, Li DC, Wang Z and Murad MH (2016) Natural language processing: use in EBM and a guide for appraisal. *Evid Based Med* **21**, 136–138.
43 Zhang X, Tang W, Chen G, Ren F, Liang H, Dang Y and Rong M (2016) An encapsulation of gene signatures for hepatocellular carcinoma, microRNA-132 predicted target genes and the corresponding overlaps. *PLoS ONE* **11**, e0159498.
44 Huang WT, Wang HL, Yang H, Ren FH, Luo YH, Huang CQ, Liang YY, Liang HW, Chen G and Dang YW (2016) Lower expressed miR-198 and its potential targets in hepatocellular carcinoma: a clinicopathological and *in silico* study. *Onco Targets Ther* **9**, 5163–5180.
45 Zamora J, Abraira V, Muriel A, Khan K and Coomarasamy A (2006) Meta-DiSc: a software for meta-analysis of test accuracy data. *BMC Med Res Methodol* **6**, 31.
46 Wang J, Ye H, Zhang D, Hu Y, Yu X, Wang L, Zuo C, Yu Y, Xu G and Liu S (2016) MicroRNA-410-5p as a potential serum biomarker for the diagnosis of prostate cancer. *Cancer Cell Int* **16**, 12.
47 Cochetti G, Poli G, Guelfi G, Boni A, Egidi MG and Mearini E (2016) Different levels of serum microRNAs in prostate cancer and benign prostatic hyperplasia: evaluation of potential diagnostic and prognostic role. *Onco Targets Ther* **9**, 7545–7553.
48 Liu L, Guo J, Yu L, Cai J, Gui T, Tang H, Song L, Wang J, Han F, Yang C *et al.* (2014) miR-101 regulates expression of EZH2 and contributes to progression of and cisplatin resistance in epithelial ovarian cancer. *Tumour Biol* **35**, 12619–12626.

49 Wang L, Li L, Guo R, Li X, Lu Y, Guan X, Gitau SC, Wang L, Xu C, Yang B *et al*. (2014) miR-101 promotes breast cancer cell apoptosis by targeting Janus kinase 2. *Cell Physiol Biochem* **34**, 413–422.

50 Zhuang C, Jiang W, Huang D, Xu L, Yang Q, Zheng L, Wang X and Hu L (2016) Serum miR-21, miR-26a and miR-101 as potential biomarkers of hepatocellular carcinoma. *Clin Res Hepatol Gastroenterol* **40**, 386–396.

51 He S, Zhang DC and Wei C (2015) MicroRNAs as biomarkers for hepatocellular carcinoma diagnosis and prognosis. *Clin Res Hepatol Gastroenterol* **39**, 426–434.

52 Varambally S, Cao Q, Mani RS, Shankar S, Wang X, Ateeq B, Laxman B, Cao X, Jing X, Ramnarayanan K *et al*. (2008) Genomic loss of microRNA-101 leads to overexpression of histone methyltransferase EZH2 in cancer. *Science* **322**, 1695–1699.

53 Xu L, Beckebaum S, Iacob S, Wu G, Kaiser GM, Radtke A, Liu C, Kabar I, Schmidt HH, Zhang X *et al*. (2014) MicroRNA-101 inhibits human hepatocellular carcinoma progression through EZH2 downregulation and increased cytostatic drug sensitivity. *J Hepatol* **60**, 590–598.

54 Liu Z, Wang J, Mao Y, Zou B and Fan X (2016) MicroRNA-101 suppresses migration and invasion via targeting vascular endothelial growth factor-C in hepatocellular carcinoma cells. *Oncol Lett* **11**, 433–438.

55 Strillacci A, Griffoni C, Sansone P, Paterini P, Piazzi G, Lazzarini G, Spisni E, Pantaleo MA, Biasco G and Tomasi V (2009) MiR-101 downregulation is involved in cyclooxygenase-2 overexpression in human colon cancer cells. *Exp Cell Res* **315**, 1439–1447.

56 Xu Y, An Y, Wang Y, Zhang C, Zhang H, Huang C, Jiang H, Wang X and Li X (2013) miR-101 inhibits autophagy and enhances cisplatin-induced apoptosis in hepatocellular carcinoma cells. *Oncol Rep* **29**, 2019–2024.

57 Lv X, Li J and Yang B (2016) Clinical effects of miR-101 on prognosis of hepatocellular carcinoma and carcinogenic mechanism of anti-miR-101. *Oncol Rep* **36**, 2184–2192.

58 Li L, Zheng BB, Ma LS, Sun X, Chang JJ, Xie WD and Li X (2014) Telekin suppresses human hepatocellular carcinoma cells *in vitro* by inducing G2/M phase arrest via the p38 MAPK signaling pathway. *Acta Pharmacol Sin* **35**, 1311–1322.

59 Yamaguchi F, Hirata Y, Akram H, Kamitori K, Dong Y, Sui L and Tokuda M (2013) FOXO/TXNIP pathway is involved in the suppression of hepatocellular carcinoma growth by glutamate antagonist MK-801. *BMC Cancer* **13**, 468.

60 Li S, Fu H, Wang Y, Tie Y, Xing R, Zhu J, Sun Z, Wei L and Zheng X (2009) MicroRNA-101 regulates expression of the v-fos FBJ murine osteosarcoma viral oncogene homolog (FOS) oncogene in human hepatocellular carcinoma. *Hepatology* **49**, 1194–1202.

61 Delire B and Starkel P (2015) The Ras/MAPK pathway and hepatocarcinoma: pathogenesis and therapeutic implications. *Eur J Clin Invest* **45**, 609–623.

62 Ye H, Zhang C, Wang BJ, Tan XH, Zhang WP, Teng Y and Yang X (2014) Synergistic function of Kras mutation and HBx in initiation and progression of hepatocellular carcinoma in mice. *Oncogene* **33**, 5133–5138.

63 Lee SY, Lee GR, Woo DH, Park NH, Cha HJ, Moon YH and Han IS (2013) Depletion of Aurora A leads to upregulation of FoxO1 to induce cell cycle arrest in hepatocellular carcinoma cells. *Cell Cycle* **12**, 67–75.

64 Dong T, Zhang Y, Chen Y, Liu P, An T, Zhang J, Yang H, Zhu W and Yang X (2017) FOXO1 inhibits the invasion and metastasis of hepatocellular carcinoma by reversing ZEB2-induced epithelial-mesenchymal transition. *Oncotarget* **8**, 1703–1713.

65 Hishida M, Nomoto S, Inokawa Y, Hayashi M, Kanda M, Okamura Y, Nishikawa Y, Tanaka C, Kobayashi D, Yamada S *et al*. (2013) Estrogen receptor 1 gene as a tumor suppressor gene in hepatocellular carcinoma detected by triple-combination array analysis. *Int J Oncol* **43**, 88–94.